nature communications

Article

https://doi.org/10.1038/s41467-024-54432-6

Cefazolin shifts the kidney microbiota to promote a lithogenic environment

Received: 22 August 2023

Accepted: 12 November 2024

Published online: 11 December 2024

Check for updates

Jose Agudelo[1,2] ✉, Xing Chen[3,4], Sromona D. Mukherjee[1], Jane K. Nguyen[5], Leslie A. Bruggeman[6,7] & Aaron W. Miller[1,8]

Clinical studies of the urinary tract microbiome, termed urobiome, suggest a direct, antibiotic-dependent, impact of the urobiome on kidney physiology. However, evidence for kidney bacteria comes from indirect sources or infected tissue. Further, it is unclear how antibiotics impact kidney bacteria. Here we show direct evidence for the presence of bacteria in the kidneys, with microniches in nephrons. In murine kidneys, administration of cefazolin, a commonly used perioperative antibiotic, led to a loss of uroprotective *Lactobacillus spp*. and proliferation of Enterobacteriaceae (which includes many known uropathogens). This effect was dependent on treatment duration, with recovery post treatment. Uroprotective *L. crispatus* and a strain of stone-associated *E. coli* differentially influenced calcium oxalate (CaOx) crystallization through the incorporation of CaOx inhibitors or promoters, respectively. In humans, microbial signatures were identified in the kidney, with unique niches between the glomeruli and tubules, established through RNA sequencing analysis and direct imaging of two independent populations. Collectively, findings support the hypothesis that the kidneys harbor a stable and antibiotic-responsive microbiota that can influence CaOx lithogenesis. The presence of unique, age-dependent microbial signatures in the glomeruli and tubuli carry implications for non-infectious kidney diseases.

Medical costs for urologic diseases account for over $11 billion in the United States annually, led by urinary tract infections (UTI) and kidney stones[1]. Urologic disease accounts for an annual global burden of 830,000 deaths and 18,467,000 disability-adjusted life years, ranking 12th among causes of death and 17th for disability[2]. Thus, continuing emphasis on understanding basic mechanisms of urologic disease is needed.

Importantly, a resident and unique urinary microbiota, or urobiome, has been described in healthy individuals, debunking long-held notions that the urinary tract is sterile[3]. Urobiome dysbiosis, driven in part by antibiotic use, has been implicated in multiple urologic diseases[4–7]. Taxa from *Lactobacillus* spp. have frequently been associated with urinary health[7–9]. One species, *L. crispatus*, has been negatively associated with urolithiasis[7,9] and has successfully been used, through vaginal administration, in clinical trials to inhibit recurrent UTIs[10]. In contrast, Enterobacteriaceae, which is a large family of Gram negative bacteria that includes uropathogenic bacteria such as *E. coli, Proteus*, and *Klebsiella*, are frequently associated with UTIs[11], kidney stone formation[7,12,13], and kidney infection (pyelonephritis)[14]. Strains of *E. coli* are recurrently identified from the

[1]Department of Cardiovascular and Metabolic Sciences, Cleveland Clinic, Cleveland, OH, USA. [2]Cleveland Clinic Lerner College of Medicine of Case Western Reserve University School of Medicine, Cleveland, USA. [3]Department of Biochemistry, School of Medicine, Case Western Reserve University, Cleveland, OH, USA. [4]Center for RNA Science and Therapeutics, School of Medicine, Case Western Reserve University, Cleveland, OH, USA. [5]Robert J. Tomsich Pathology and Laboratory Medicine, Diagnostics Institute, Cleveland Clinic, Cleveland, OH, USA. [6]Department of Inflammation and Immunity, Cleveland Clinic, Cleveland, OH, USA. [7]Department of Kidney Medicine, Cleveland Clinic, Cleveland, OH, USA. [8]Department of Urology, Cleveland Clinic, Cleveland, OH, USA. ✉e-mail: agudelj@ccf.org

nidus and periphery of CaOx stones, suggesting a non-random entrapment of these microbes into stones that are considered as "metabolic"[15]. Additionally, some strains isolated from CaOx stones have shown to enhanced crystallization potential[7,16,17].

While the presence of upper urinary tract bacteria has been implied through analysis of kidney stones, voided urine samples, and renal pelvis urine, direct evidence of a resident microbiota in the kidneys is lacking. Bacteria isolated from non-infectious stones are unique from taxa identified in the lower urinary tract (LUT)[7,16]. However, bacteria in kidney urine are not significantly different from midstream-voided urine[16]. Recent analysis of micro-dissected tubuli and glomeruli RNA sequencing (RNAseq) data show unique microbial RNA signatures in each compartment, with significant differences in composition based on kidney function and disease[18]. Collectively, data provide strong circumstantial evidence of a kidney microbiota that may be influenced by antibiotics and impacts kidney health, which warrants further investigation.

In the current study, we aimed to determine the presence and impact of antibiotics on renal microbiota in a mouse model and understand the mechanisms of lithogenesis for uroprotective *L. crispatus*[7,9] and stone-associated strain of *E. coli* (ATCC 43886), which is the most abundant species present across multiple stone types[7,13,15,17]. Finally, we sought to validate the presence of kidney microbiota in humans, using molecular and imaging techniques.

Here, we show a low biomass microbial community present in microniches of the kidneys in human and mice, with a pattern of disturbance caused by antibiotics that suppresses Lactobacillus taxa, and proliferates Enterobacteriaceae. An in vitro lithogenic model shows that stone-associated and antibiotic resistant *E. coli* was associated with enhanced lithogenesis, while antibiotic susceptible *L. crispatus* was associated with inhibition of crystallization metrics. These findings suggest that the renal microbiome may play a role in either preventing or promoting CaOx lithogenesis based on antibiotic disturbance.

Results

Mice kidneys harbor a unique microbial signature

Given pragmatic issues in establishing and assessing a kidney microbiota in humans, comprehensive assessment of the kidney microbiota was initially examined in mice. To quantify viable bacterial loads in mouse kidneys, aseptically retrieved punch biopsies of three, 10-week-old SWR/J mice housed in a clean barrier facility were plated undiluted in seven different media, incubated, and colony-forming units (CFUs) quantified. Data revealed a significant increase in bacterial density from the renal cortex to medulla, then ureter (Fig. 1a,b; Paired chi-square $x^2 = 5.024$, $p = 0.023$ (a) or t-test cortex:medulla- $t = 3.96$; $p = 0.0036$; cortex:ureter- $t = 6.47$; $p = 0.00002$; ureter:medulla- $t = 2.17$; $p = 0.09$ (b)). Negative controls did not produce CFUs. An RNA-targeted, fluorescence in situ hybridization (FISH) analysis of kidneys stained with a universal probe for bacteria shows the presence bacteria in the medulla and cortex (Fig. 1c) and is consistent with the distribution of bacteria assessed by culture-based means.

To evaluate the presence of a kidney microbiota using criteria established for low biomass microbial communities[19] and quantify the impact of antibiotics on kidney bacteria, one-hundred sixty SWR/J mice were exposed to antibiotics, with or without recovery, in parallel with non-exposed controls (Fig. 1). Animals exhibited an antibiotic-dependent difference in water intake and urine output similar to past studies[20], but not food intake or body mass (Two-way ANOVA and post-hoc, Holm's corrected, paired t-tests; $t = 16.436$, $p < 0.001$ for water, $t = 10.23$ $p = 0.001$ for urine; Fig. 2). A total of 239 urine samples and 40 kidneys were subjected to high-throughput sequencing of the V4 region of the *16S rRNA* gene. There was an average of 8336 + /- 598 reads per sample, with 2821 + /- 62 mapping to host reads. Kidney and urine samples were significantly different than positive and negative controls in terms of microbial community composition (Permanova $f = 3.98$, $p = 0.001$; Fig. 3a). All kidney and urine samples surpassed the sequencing threshold to provide a statistically representative snapshot of microbial communities based on rarefaction analysis, defined as the sequencing depth that >90% of samples had a slope of <0.01 (Fig. 3b). While 5.34% of high-quality reads were removed from urine samples as Eukaryotic/host, 52% of reads were removed from kidney specimens as Eukaryotic/host (ANOVA, $f = 5.73$, $p < 0.001$; Fig. 3c).

PERMANOVA analysis, based on weighted UniFrac dissimilarity, revealed that the murine kidneys and urine microbiomes were unique ($f = 97$, $p = 0.001$; Fig. 1d). Taxa in kidneys and urine were dominated by the Pseudomonadota and Bacilliota, with relatively high numbers of Actinobacteriota and low levels of Bacteroidota (DESeq2; FDR < 0.05 for significantly different phyla; Fig. 1e), consistent with voided human urine[7,9,21,22] and in contrast to predominant taxa in murine stool[23]. We detected significantly higher species richness/evenness in urine compared to kidneys (paired t-test; PD_whole_tree $t = 3.24$, $p = 0.19$; Margalef $t = 914$, $p = 0.0009$; Shannon $t = 2.7 \times 10^{11}$, $p = 6.9 \times 10^{-12}$; equitability $t = 4.5 \times 10^{17}$, $p = 5.6 \times 10^{-18}$; Fig. 1f). *Acinetobacter*, a common urobiome taxon[22], was most enriched in urine compared to kidneys (DESeq2; FDR < 0.05 for significantly different taxa; Fig. 1g, Supplementary data S1). *Pseudomonas* was most enriched in kidneys, compared to urine (Fig. 1g), a taxon that is resident in other organs, such as lung tissue[24].

Importantly, vesicoureteral reflux (VUR) assays[25] were conducted in 12-weeks male SWR/J to assess this renal defect phenotype in this breed used for the experiment. (Fig. 1h). Five animals were tested under the protocol described in the methods, and not any reflux was recorded from 30 to 150 cm^2, observing exit of dye through the urethra at the highest pressure.

Long-term use of cefazolin impacts the LUT of mice, with recovery

Long-term use of cefazolin had a significant impact on bacterial composition and richness of the urine, even with a recovery period (2-way Anova $f = 12.6$, $p = 0.0007$; Fig. 2a; 2-way Anova $f = 8.5$, $p = 0.021$; Fig. 2b; Permanova $f = 3.94$, $p = 0.018$; Fig. 2c). Short-term antibiotic exposure did not impact the composition or richness (2-way Anova $f = 0.014$, $p = 0.909$; Fig. 4a; 2-way Anova $f = 4.064$, $p = 0.05$; Fig. 4b; Permanova $f = 0.98$, $p = 0.32$; Fig. 4c).

To identify taxa positively or negatively impacted by antibiotic treatment in urine samples, we conducted a differential abundance analysis of amplicon sequence variants (ASVs) in animals that received a long-term course of antibiotics from baseline to the last day of exposure, compared to non-exposed controls (DESeq2, FDR < 0.05 Fig. 2d, Supplementary data S2). Genera of known uropathogens *Pseudomonas* (8 ASV's), *Proteus* (6 ASV's), and *Enterococcus* (10 ASV's) significantly increased in abundance with antibiotic use ($p < 0.01$), indicative of antibiotic resistance, whereas Planococcaceae (7 ASV's), Bacilliales (32 ASV's), *Staphylococcus* (6 ASV's), and *Lactococcus* (9 ASV's) were most negatively impacted by intervention (FDR < 0.05). With the exception of *Staphylococcus*, infections by these taxa are rare and instead may represent the commensal urinary flora. *Acinetobacter* (19 ASV's) most benefitted from time in the trial without antibiotic use (FDR < 0.05).

Previous studies suggest that bacteria from the Enterobacteriaceae and *Lactobacillus* taxa, present in kidney stones and urine, are associated with pro- or anti-lithogenic influences, respectively, on kidney stone development[7,9,15]. As such, we sought to evaluate the susceptibility of these specific taxa to antibiotic disturbance, as the use of antimicrobials have been associated with the development of stones[7,26]. *Proteus*, a causative agent of UTIs and struvite stones[27], is from the Enterobacteriaceae family and was one of the taxa that increased in abundance most after antibiotic use (6 ASV's, FDR < 0.05), while *Lactobacillus* was significantly inhibited by antibiotics (Fig. 2d). Molecular and culture-based analysis of all Enterobacteriaceae and *Lactobacillus* at the endpoint for all groups, revealed that there was no

https://doi.org/10.1038/s41467-024-54432-6

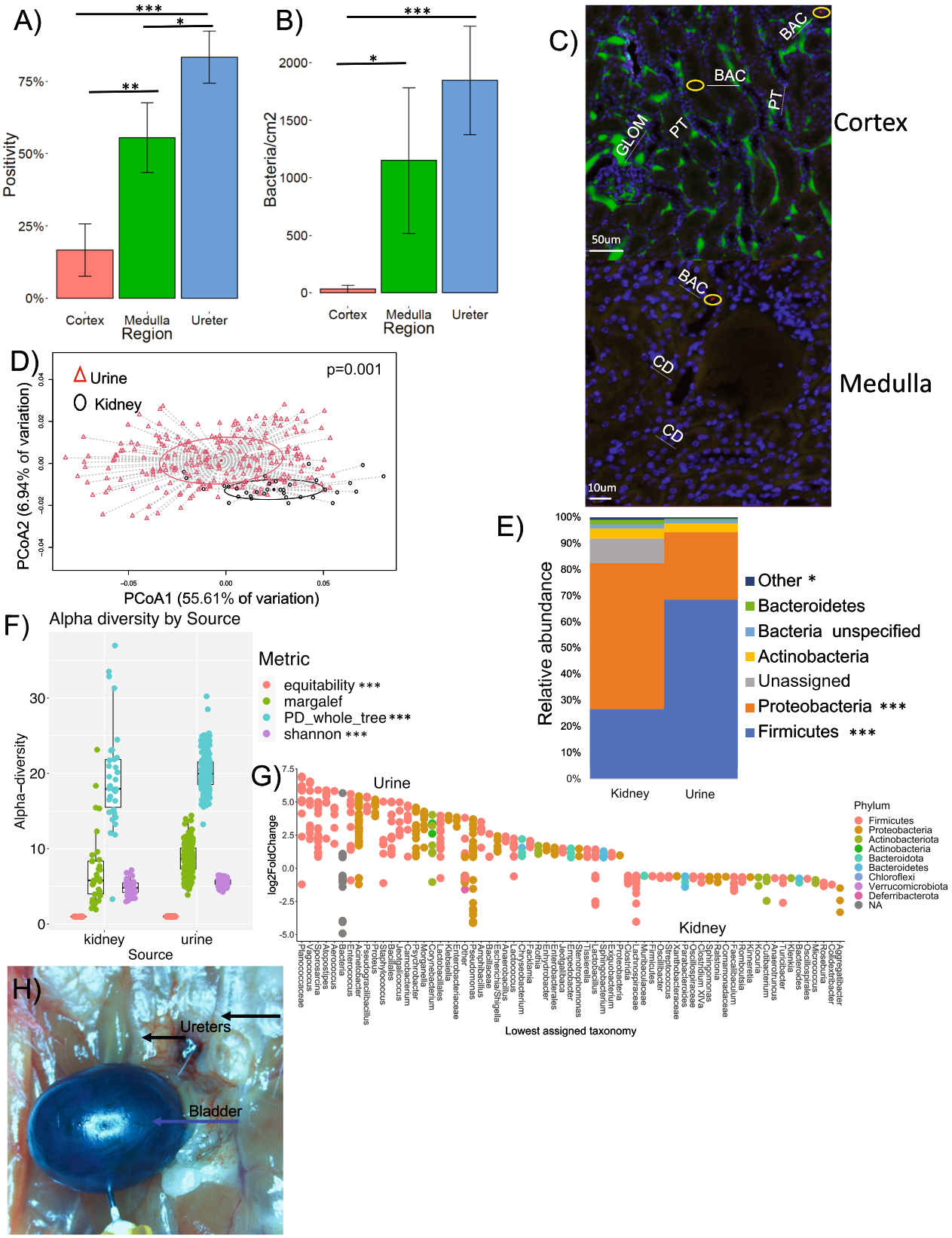

impact of antibiotics on the Enterobacteriaceae, but a significant reduction of *Lactobacillus* (Two-way ANOVA f = 2.097, $p = 0.04$; Fig. 2e, f = 10.665, $p = 0.013$; Fig. 4d). Antibiotic-associated dysbiosis is consistent with published clinical urobiome data[7,28,29] as well as antibiotic sensitivity testing across multiple *Lactobacillus*[30] and Enterobacteriaceae[31] species.

Proteomic techniques have revealed an upregulation of proinflammatory cytokines in the kidneys and urine of stone formers[32]. In our study, we observed a significant, antibiotic-associated increase in the urinary cytokines IL-1β and IL-6, but not IL-18 (Two-way ANOVA, f = 16.49, $p = 0.002$; Fig. 2f), which could reflect urinary dysbiosis-driven inflammation due to higher levels of Enterobacteriaceae[33] or an

Fig. 1 | Composition and distribution of kidney bacteria in mice. A Proportion of positive regions in kidney biopsies (undiluted) exhibiting at least one bacterial colony after inoculation of kidney tissue on six different culture media. $N = 18$/segment. Paired, Holm's corrected, paired chi-square tests; cortex:medulla-df=53; $X^2 = 5.024$; $p = 0.023$; medulla:ureter; $X^2 = 5.024$; $p = 0.026$; ureter:cortex; $X^2 = 10.234$; $p = 0.00004$. **B** Microbial density in kidney biopsy by regions (bacterial cells/cm^2), from six different culture media. $N = 18$/segment. Paired, Holm's corrected, paired t-tests; cortex:medulla-df=53; t = 3.96; $p = 0.0036$; cortex:ureter-df=53; t = 6.47; $p = 0.00002$; ureter:medulla -df=53 t = 2.17; $p = 0.09$. **C** Hybridization of FISH bacterial probe in both the cortex and medulla showing proximal tubules (PT), glomeruli (GLOM), DAPI-stained nuclei (blue color), and bacteria stained with the universal, EUB probe (BAC, red dot within yellow circle). Green fluorescence is auto-flourescence. Representative image was repeated for 5 animals in the LT_abx group and 5 in the LT_noabx group. All data generated from these images is presented in Fig. 3C. **D**–**G** Comparison of bacterial diversity using *16S rRNA* V4 region sequencing from animals of all the experimental groups independent of intervention. **D** Principle component analysis (PCoA of weighted UniFrac distance between kidney and urine samples. Statistical analysis was conducted as a PERMANOVA with 999 permutations (N = 34 kidneys, 267 urine; df=300; f = 97; $p = 0.001$). **E** Comparative phylum profile between kidney and urine samples. Statistical comparison is provided by a false discovery corrected, DESeq2 differential abundance at the phylum level. Statistical analysis was a DESeq2 differential abundance (N = 34 kidneys, 267 urine; FDR < 0.05 for phyla with *) **F** Alpha diversity of normalized samples using different metrics. Statistical significance is provided by Holm's-corrected, paired t-tests (N = 34 kidneys, 267 urine; df = 300; PD_whole_tree t = 3.24, $p = 0.19$; Margalef t = 914, $p = 0.0009$; Shannon t = 2.7×10^{11}, $p = 6.9 \times 10^{-12}$; equitability t = 4.5×10^{17}, $p = 5.6 \times 10^{-18}$. **G** Differential abundance of taxa between kidney and urine. Statistical significance is provided by false discovery corrected, DESeq2 differential abundance at the ASV level. Taxa are listed to lowest assigned taxonomy. All listed taxa have FDR < 0.05. Positive log2foldchange represents ASV's enriched in urine, negative values are ASV's enriched in kidneys. The full set of significantly different ASVs is provided in Supplementary data 1. **H** Blue arrow shows the bladder, filled with methylene blue at 150 cm^3 of pressure. Black arrows show the ureters with no blue dye. *p-value < 0.05, **p-value < 0.01, ***p-value < 0.001. For box and whisker plots; the center is the data mean, minima and maxima are the 25th and 75th percentiles; whiskers extend 1.5 interquartile range from minima and maxima. Source data are provided as a Source Data file.

oxalate-driven inflammatory response due to reduced oxalate degradation[34,35].

Murine kidney microbiota is stable, but shifts towards uropathogenic bacteria with cefazolin exposure

To evaluate the stability of the murine renal microbiota, we quantified alpha diversity of the kidney microbiome longitudinally for animals not exposed to antibiotics, similar to previous analyses in low microbiome echosystems[36]. While antibiotic exposure did not significantly change the number of microbial species detected in the kidneys (paired t-test, t = 0.5, $p = 0.6$' Fig. 3a), there was a shift in overall microbial composition based on weighted UniFrac dissimilarity (Permanova, f = 3.94, $p = 0.03$; Fig. 3b). In contrast, there was no impact of a short-term course of antibiotics for the kidney microbiome (Fig. 4e; one-way ANOVA, $N = 4$-6/group, df=9, f = 0.03 for Abx; $p = 0.867$; Fig. 4f; Permanova, $N = 4$-5/group; df=8, f = 1.153,$p = 0.654$). There were no significant changes in renal microbial alpha diversity over 30 days (Pearson's correlation, r = 0.14, 0.45, 0.5, 0,42 and $p = 0.6$, 0.2, 0.16, 0.2 for equitability, Margalef, PD_whole_tree, and Shannon; Fig. 3c), indicative of a stable community[37]. Similar to the LUT, *Acinetobacter*, *Lactobacillus* and *Lactococcus* (1 ASV each) were lost in the kidneys with antibiotic treatment (DESeq2; FDR < 0.05). *Tepidimonas* and *Lysinibacillus* (1 ASV each) proliferated with antibiotic administration (Fig. 3d, Supplementary data S3; FDR < 0.05). There was no effect of a short-term course of antibiotics on species number or composition (paired t-test, t = 0.03, $p = 0.867$; Fig. 4e).

To validate molecular data, an RNA-FISH protocol was utilized to localize and quantify microbial DNA through hybridization in mouse kidney tissue. Three targeting probes were used for all bacteria, Enterobacteriaceae, or *Lactobacillus*. The protocol was validated with pure cultures from either the Enterobacteriaceae or *Lactobacillus* taxa, isolated from mouse urine (Fig. 5a–c). The EUB (universal), PB (Enterobacteriaceae) and GC (*Lactobacillus*) probes hybridized to the intended targets of all bacteria, Enterobacteriaceae, and *Lactobacillus*. There was co-localization with DAPI signals with all probes, and no cross hybridization observed in triplicate samples. Kidney slides stained with DAPI and any one of the three probes exhibited bacterial signals primarily located in the medulla, in or around the renal tubules and collecting ducts (Fig. 5d–f). Negative controls, which included stained slides without tissue or bacteria (Fig. 5g) did not exhibit any bacterial signals. Additionally, serial sections of mice kidney samples stained with randomly scramble probe sequences did not exhibit fluorescent signals, compared to their counterpart sections from the same samples stained with bacterial targeting probes (Fig. 5h–j). Quantitative analysis of bacteria was independently performed by two analysts blinded to sample identifiers. Analysis of surroundings and borders of kidney tissue did not show the presence of randomly distributed bacteria, suggesting no contamination during slide processing[38]. Histologic analysis revealed no indications of calcium oxalate deposition or kidney injury. Quantitative results show a significant loss of total microbial density in the kidneys with antibiotics (paired t-tests, t = 12.69 $p = 0.04$), with a clear impact on *Lactobacillus* (t = 9.81, $p = 0.04$), but not on Enterobacteriaceae (t = 0.04, $p = 0.316$; Fig. 3e), consistent with molecular (Figs. 2e, 3d) and culture-based (Fig. 4d) analyses in urine. These findings suggest a shift in kidney microbial communities caused by antibiotics towards antibiotic-resistant, uropathogenic Enterobacteriaceae and away from uroprotective bacteria such as *Lactobacillus*. Validation of results were obtained through antibiotic resistance assays on a kidney stone-associated strain of *E. coli* (ATCC 43886)[7,13] and a strain of *L. crispatus* that is negatively associated with urinary stone disease[7–9,39], such that *L. crispatus* was significantly more susceptible to three out of four antibiotics tested compared to *E. coli* (Fig. 3f; $p = 0.02$). Genomic analysis revealed that the genome of *E. coli* (ATCC 43886) harbors more antibiotic resistance genes than *L. crispatus* (Fig. 6a).

Occasional outbreaks of Enterobacteriaceae hybridization in the kidneys were apparent and clusters were often observed (Fig. 3g). These observations were consistent with molecular data which saw three of the 10 mice exhibiting very high Enterobacteriaceae counts compared to the other animals (Fig. 6b), which may result from virulence factors, as suggested by the higher number of genes for biofilm formation, stress response, and competition than *L. crispatus* (Fig. 6a). Molecular comparison of Enterobacteriaceae and *Lactobacillus* in the kidneys, reveals that either one or the other taxa was dominant, indicative of potential direct competition (Fig. 6c).

Specific strains of *Lactobacillus* and *E. coli* compete and differentially impact calcium oxalate crystal metrics through known non-canonical pathways

To determine the direct impact of candidate bacteria on the growth of calcified crystals, we utilized a CDC bioreactor system, which is a specialized chemostat that mimics the constant flow, shear forces, temperature, and biochemical environment of the kidneys, while providing a removable surface for biofilm growth[40]. Uroprotective *L. crispatus* and stone-associated strain of *E. coli* (ATCC 43886) were incubated in the bioreactor individually and in co-culture to evaluate their influence on CaOx crystallization.

Artificial urine media (AUM; Supplementary data S4) was run at a constant flow into the chemostat system, which was placed on a stir plate at 37 °C and at a constant stir rate. The system was either run

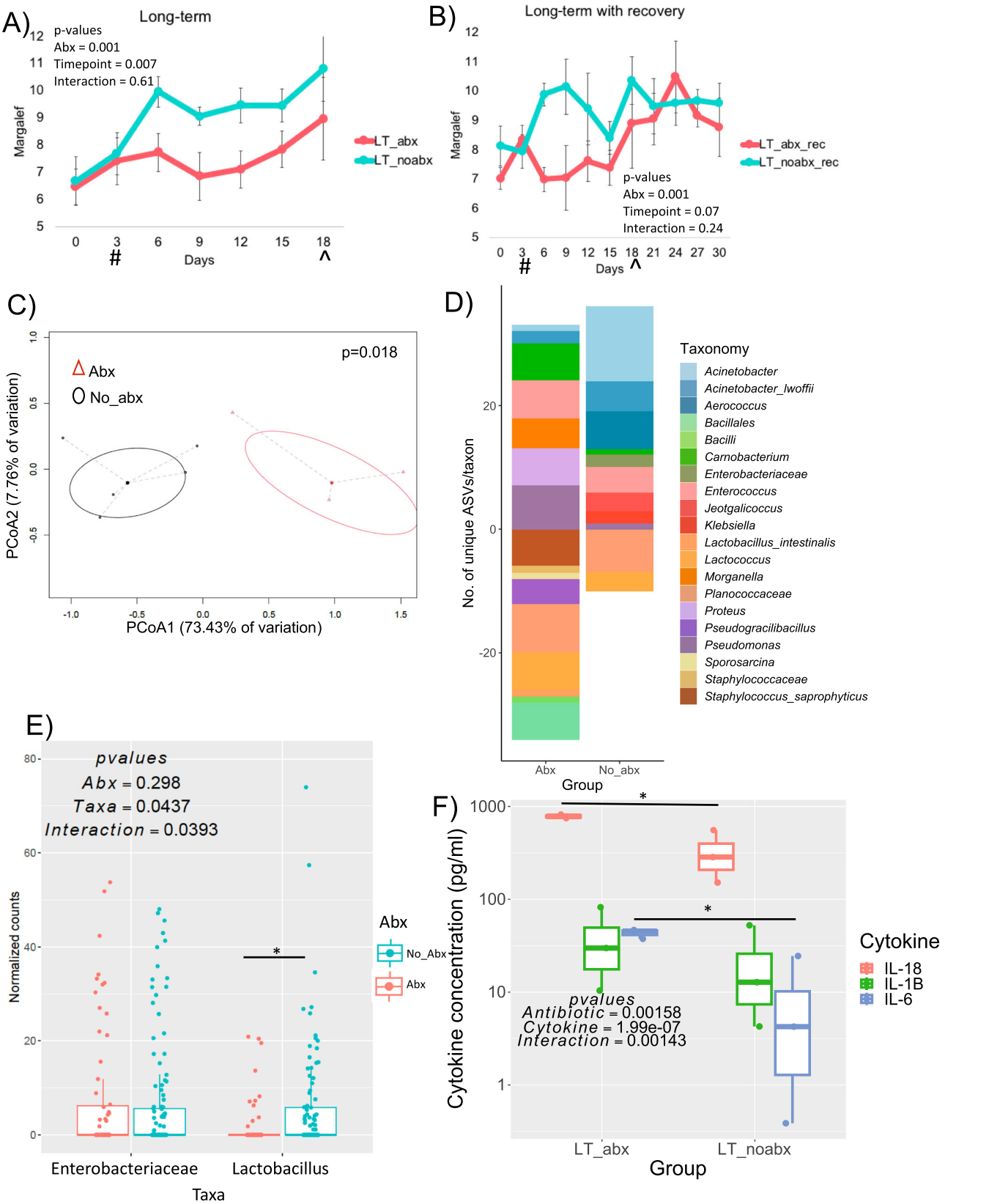

sterile or inoculated with candidate bacteria at equal starting densities. After 72hrs, removable polycarbonate coupons were analyzed with scanning electron microscopy (SEM) and energy dispersive x-ray spectroscopy (EDS). Aliquots of media from each experiment were used to quantify bacterial density and viability. No culturable bacteria were recovered from sterile controls. For SEM and EDS, a pure, clinically extracted CaOx stone was included for crystal morphology analysis, along with in vitro CaOx crystals for validation of bioreactor studies.

In qRT-PCR analysis, when grown alone, 100% of sequences were attributed to *E. coli* or *L. crispatus*, relative to a universal bacterial primer (paired t-test against *L. crispatus*, t = 7.173, 8.459 and

Fig. 2 | Impact of cefazolin on urine microbiota. A Alpha diversity (Margalef's species richness) over the course of the experiment for animals given cefazolin long-term and controls with no antibiotic treatment. Two-way ANOVA results are shown. Means are plotted +/- SEM. (N = 3-5 per group/timepoint; df=61; f = 12.6, 15.67, and 2,55 for group, timepoint, and interaction; $p = 0.0007$, 0.0002, and 0.11, respectively. **B** Alpha diversity over the course of the experiment for animals given cefazolin long-term and controls with no treatment, and with recovery following antibiotic cessation. Two-way ANOVA results are shown. Means are plotted +/- SEM. (N = 3-5 per group/timepoint; df=99; f = 8.5; $p = 0.021$. #Indicates when antibiotics started. ^Indicates the point at which antibiotics ceased. **C** PCoA of weighted UniFrac distance between the last timepoint for urine specimens with long-term antibiotic use (LT_abx) and controls without antibiotics (LT_noabx). Statistical comparison was conducted as a PERMANOVA with 999 permutations (N = 5/group; df=7, f = 3.94,$p = 0.018$). **D** Differential abundance taxa between the first and the last timepoints in urine specimens with or without antibiotic exposure. Negative values are the number of taxa lost over the course of the trial, while positive values are those that increased in abundance. Statistical significance is provided by false discovery corrected, DESEQ2 differential abundance at the ASV level. Taxa are listed to lowest assigned taxonomy. $N = 5$/group. Full set of significant results and statistics is provided in Supplementary data 2. **E** Impact of cefazolin on the abundance of *Lactobacillus* and Enterobacteriaceae, based on *16S rRNA* sequencing of all animals. 2-way ANOVA results are shown (N = 132/group; df=342, f = 1.088, 2.097, and 4.281 for abx, taxa, and interaction; $p = 0.29$, 0.04, and 0.04, respectively. **F** Urinary cytokine concentrations (by ELISA) in response to long-term antibiotic use. Two-way ANOVA results are shown with post-hoc paired, Holm's-corrected t-tests. (N = 3/group; df = 17, f = 16.49, 72.51, and 11.87 for abx, cytokine, and interaction; $p = 0.0016$, 1.99×10^{-7}, and 0.001, respectively. *p-value < 0.05, **p-value < 0.01, ***p-value < 0.001 for post-hoc t-tests. # indicates start of antibiotics; ^ indicates antibiotic cessation. For box and whisker plots; the center is the data mean, minima and maxima are the 25th and 75th percentiles; whiskers extend 1.5 interquartile range from minima and maxima. Source data are provided as a Source Data file.

$p = 0.0003$, 0.0002 for co-cultures and *E. coli;* Fig. 7a; paired t-test against *L. crispatus*, t = 8.54, 9.76 and $p = 0.0009$, 0.0005 for co-cultures and *E. coli;* Fig. 7b). When co-cultured, *E. coli* (ATCC 43886) comprised ~90% of the culture after three days, despite equal inoculation densities (Fig. S7a, b). No detectable DNA was recovered with qRT-PCR from sterile controls. The *E. coli* strain (ATCC 43886) exhibited significantly higher viability compared to *L. crispatus*, in pure culture. However, the proportion of viable bacteria was significantly reduced in co-culture (ANOVA, f = 52.81, $p = 0.0002$; Fig. 7c). The more effective competitiveness by *E. coli* (ATCC 43886) was also reflected in the number of genes for competition in genome analyses (Fig. 6a).

The CaOx crystals were styloid laminated sheets in a clinical pure CaOx stone (Fig. 4a), consistent with CaOx monohydrate[41], which is generally found on the surface of CaOx stones. In sterile media, crystals exhibited an octahedral structure, consistent with CaOx dihydrate crystals (Fig. 4b)[42]. Additionally, spherical structures less than 1µm in diameter were common, which appeared to aggregate into amorphous, then octahedral structures (Fig. 4b), consistent with a recently reported, non-canonical pathway for CaOx crystallization and growth[43]. To confirm abiotic origins of these nanospheres, we filter sterilized fresh AUM and observed media under light microscopy after one hour. Imaging showed a few shapes compatible with CaOx dihydrate crystals, but also showed many of the styloid crystal shapes and nano-sized spheres that were the same size and shape as those observed in SEM analysis (Fig. 7d). No culturable bacteria were recovered from this media, similar to sterile bioreactor runs. When stone-associated strain of *E. coli* (ATCC 43886) was grown by itself, octahedral structures were abundant along with nanospheres that appeared to aggregate to octahedral crystals (Fig. 4c). Bacteria were often found attached to octahedral structures. In contrast, when *L. crispatus* was grown alone, only small, amorphous crystal structures formed, with no bacterial attachment (Fig. 4d). When *E. coli* (ATCC 43886) and *L. crispatus* were co-cultured, styloid, CaOx monohydrate crystal structures were observed (Fig. 4e), indicative of an entirely different microbe-crystal interaction. Quantification of crystal size in bioreactor studies showed *E. coli* (ATCC 43886) grown alone produced the largest crystals, followed by sterile media, then *L. crispatus* grown alone (ANOVA, f = 52.54, $p < 0.001$; Fig. 4f). However, the influence on crystallization, based on plate-based crystal size assays, of other ATCC purchased species of lactic-acid bacteria and different strains of *E. coli* isolated from calcium-based stones was different from the findings observed with the bioreactor experiments. (ANOVA, f = 78.97, $p < 0.001$; Fig. 4g). Collectively, data suggest that this strain of *E. coli* (ATCC 43886) facilitates the growth and aggregation of CaOx crystals into larger and more complex octahedral structures through a non-canonical pathway, whereby CaOx nanospheres aggregate into amorphous structures and continue aggregating until the octahedral structures develop and further aggregate[44]. In contrast, *L. crispatus* appears to inhibit this process at the amorphous phase.

The differential interaction between bacteria and CaOx crystallization could either be mediated through oxalate production/degradation, by the production of pro-/anti-lithogenic molecules, or by the interaction of proteins on the bacteria surface on crystal faces[15]. Genome analysis revealed that both species have an equal number of oxalate metabolism genes (Fig. 6a). A previous report showed that healthy individuals had a higher abundance of *L. crispatus* oxalate-degrading genes in their urine compared to CaOx stone formers[9]. In vitro oxalate-degrading assays revealed that *L. crispatus* was able to degrade significant amounts of oxalate, confirming genome and metagenomic analyses, but the stone-associate *E. coli* (ATCC 43886) produced significant amounts of oxalate (Two-way ANOVA, f = 23.47, $p < 0.001$; Fig. 7e).

Genome analysis revealed that *E. coli* (ATCC 43886) harbors more genes that overlap with known lithogenic factors, compared to *L. crispatus*, which includes genes for urea and metal interactions (Fig. 6a). In an energy dispersive x-ray spectroscopy (EDS)-based assay, peaks of calcium, carbon, and oxygen were observed in crystals formed by *E. coli* (ATCC 43886) and *L. crispatus*, consistent with CaOx crystals (Fig. 5a). The largest CaOx peaks were observed in the clinically extracted stone, along with the crystals from the sterile and *E. coli* (ATCC 43886) experiment. Other elements were present in lower abundance, such as sodium, chloride and nitrogen. Binomial dissimilarity matrix analysis of the whole elementome revealed treatment-specific effects with significant differences based on the presence or absence of bacteria (Permanova, f = 4.85, $p = 0.001$; Fig. 5b, ANOVA, f = 1.47-3.83, $p = 0.004$-0.206; Fig. 8a–h). Crystals that developed when *L. crispatus* was present were enriched in sulfur (Fig. 8f) and phosphorus (Fig. 8h), known calcium competitors linked to lower CaOx urolith formation[44–48]. In contrast, crystals formed when *E. coli* (ATCC 43886) was present were enriched in chloride (Fig. 8g) and iron (Fig. 8c), known promoters of CaOx crystals[49–51].

Metagenomic and FISH data from human renal specimens show microbial signature differentiated by tissue proximity, age, and ethnicity

To evaluate the presence of microbial signatures in human renal specimens, we conducted an RNA-FISH analysis of kidney biopsies and autopsies, using the universal bacterial probe (EUB). Image analysis revealed bacteria in all samples, typically reserved to lumen spaces (Fig. 6a-d). Bacterial density, estimated as the relative area of bacterial stain compared to total kidney tissue, was not significantly different between biopsies and autopsies, which suggests that bacterial proliferation post-mortem did not contribute to bacterial signals (paired t-test, t = 2.195, $p = 0.177$; Fig. 6e).

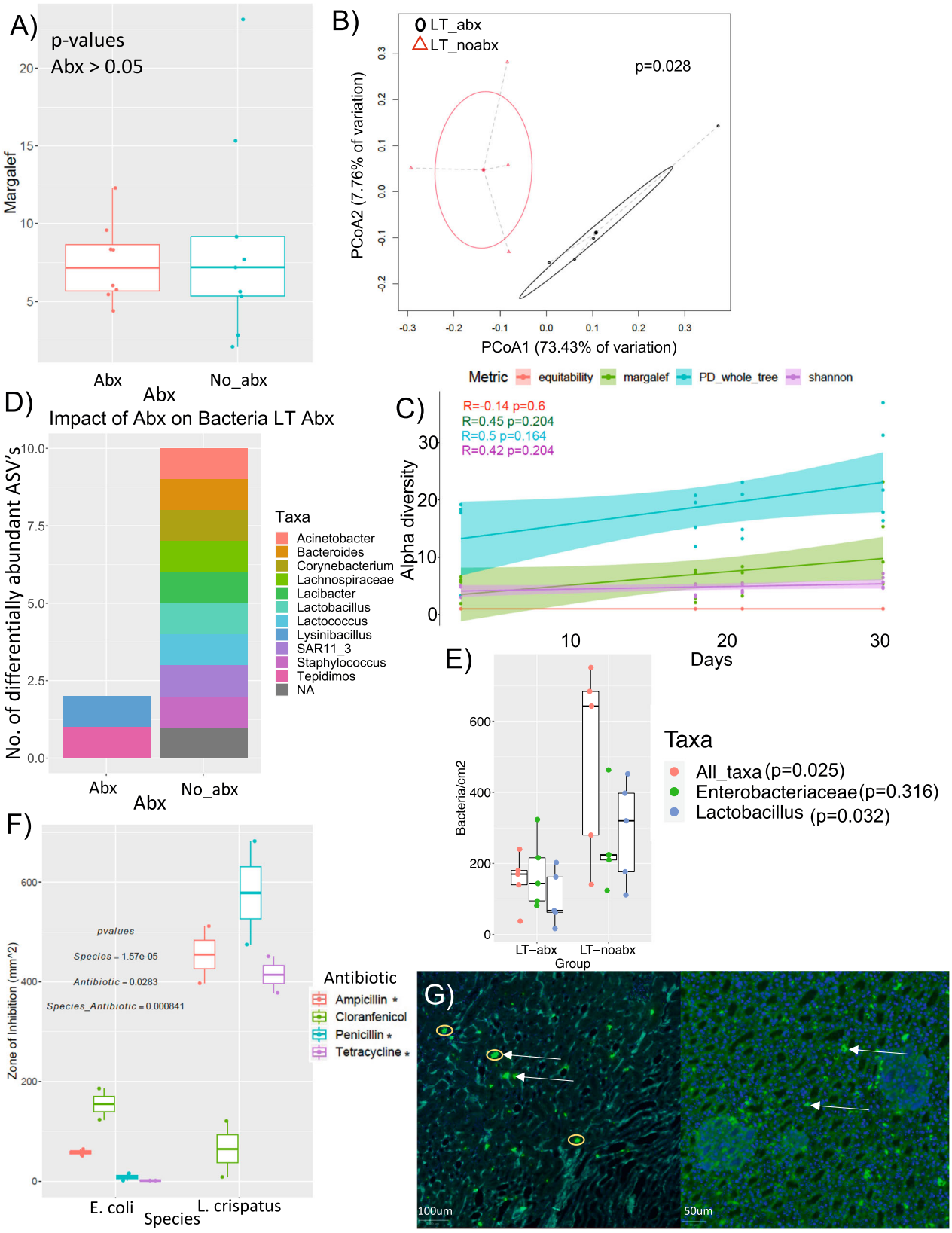

To further evaluate the presence of bacteria in human kidneys, bacterial signatures in an independent population of kidney specimens were re-analyzed from a previously published transcriptomic dataset of micro-dissected glomeruli and tubuli that underwent polyA enrichment prior to sequencing (BioProject PRJNA725213)[52]. There were 101 sequenced samples from healthy participants available, which included 71 glomeruli and 30 tubuli. There was an average of 38,646,509 +/− 1,301,280 total reads/sample, with 19,086,347 +/− 639,898 mapping to host reads, and 56,191 +/− 2934 mapped to prokaryotes after removal of potential contaminants and low-quality reads. We observed significant differences in the ratio of high-quality sequences mapping to prokaryotes vs. human reads between

Fig. 3 | Impact of cefazolin on kidney microbiota. A Alpha diversity (Margalef's species richness) of the kidney microbiota post-necropsy for animals given cefazolin long-term and controls with no antibiotics. P-value reflects a paired t-test (N = 8-9/group, df=16, t = 0.505, $p = 0.6$. **B** PCoA of weighted UniFrac distance between the last timepoint for kidney specimens with long-term antibiotic use (LT_abx) and controls without antibiotics (LT_noabx) (N = 3-5; df=6, f = 3.94, $p = 0.028$). Statistical analysis was conducted as a PERMANOVA with 999 permutations. **C** Alpha diversity of the kidney microbiota post-necropsy for animals not exposed to cefazolin, sampled at different time points, for multiple alpha diversity metrics. Statistical analysis is based on Pearson correlations between alpha diversity and time in animal study. ($N = 17$; df=6; r = -0.14, 0.45, 0.5, and 0.42 for equitability, margalef, PD_whole_tree, and Shannon; $p = 0.6$, 0.068, 0.041, and 0.09, respectively. **D** Differential abundance of taxa between kidneys from mice given cefazolin long term or controls with no antibiotics. Statistical significance is provided by false discovery corrected, DESeq2 differential abundance at the ASV level. Taxa are listed to lowest assigned taxonomy. $N = 5$/group, df=68. Full set of significant results and statistics is provided in Supplementary data 3. **E** Effect of a long-term course of antibiotics on all bacteria, Enterobacteriaceae, and *Lactobacillus sp.*, based on direct counts of FISH-stained bacteria in the cortex and medulla of kidney sections. ANOVA results are shown with post-hoc paired, Holm's-corrected t-tests. (N = 5/group; df=29; t = 12.69, 0.65, and 9.81 for all bacteria, Enterobacteriaceae, and Lactobacillus; $p = 0.04$, 0.316, 0.04, respectively. **F** Validation of differential antibiotic susceptibility of *Lactobacillus* sp. and Enterobacteriaceae with the use of susceptibility testing discs, using pure cultures of *L. crispatus* (ATCC 33197) and *E. coli* (ATCC 43886). Two-way ANOVA results are shown with post-hoc paired, Holm's-corrected t-tests. (N = 2/species, antibiotic due to low variance and strong effect sizes; t = 15.5, 0.74, 10, and 41 for Ampicillin, Choranfenicol, Penicillin, and Tetracycline, $p = 0.04$, 0.3, 0.04, 0.028, respectively. **G** FISH-based imaging of an outbreak of Enterobacteriaceae. White arrows indicate fluorescently labeled Enterobacteriaceae. Yellow circles highlight clusters of individually discernable bacteria. Left image is the outer medulla, populated largely be distal tubules and the right image is the cortex, populated largely by proximal tubules. Representative image was repeated for 5 animals in the LT_abx group and 5 in the LT_noabx group. All data generated from these images is presented in Fig. 3C. *p-value < 0.05, **p-value < 0.01, ***p-value < 0.001 for post-hoc t-tests. For box and whisker plots; the center is the data mean, minima and maxima are the 25th and 75th percentiles; whiskers extend 1.5 interquartile range from minima and maxima. Source data are provided as a Source Data file.

glomeruli and tubuli (paired t-test, t = 26.99, $p < 0.001$; Fig. 9a). Importantly, nearly all reads exhibited 100% sequence homology with their microbial references, which minimizes the possibility of false microbial annotations (Fig. 9b). Wih this analysis, we observed significantly greater species richness in the glomeruli compared to tubuli (paired t-test, t = 25.37, $p = 0.0007$; Fig. 9c), with a posititve correlation with increasing age (Pearson's correlation, r = 0.43, -0.14 and $p = 0.0003$, 0.45 for glomeruli and tubuli; Fig. 9d). The composition of the microbial signatures was significantly different between the glomeruli and tubuli, assessed with a Bray-Curtis dissimilarity index (Permanova, f = 28.58, $p = 0.001$; Fig. 9e). Bacterial phyla indentified in glomeruli and tubuli were dominated by Pseudomonadota and Bacilliota (Fig. 9f), consistent with previous urobiome studies[7,21]. Taxa that differentiated the glomeruli and tubuli, based on a DESeq2 analysis, were primarily *Streptomyces* (38 ASV's), *Pseudomonas* (22 ASV's), *Burkholderia* (16 ASV's), and *Streptococcus* (15 ASV's) in the glomeruli and *Bacillus* (17 ASV's) in the tubuli (DESeq2, FDR < 0.05; Fig. 9g; Supplementary data S5). Similar results were obtained with an ANCOM analysis (ANCOMBC, FDR < 0.05; Fig. 9h). Ethnicity was a significant driver of composition and species richness in two-way analyses (Permanova, f = 2.85, $p = 0.007$; Fig. S9i; ANOVA, f = 6.191, $p = 0.0007$; Fig. 10a). We did not see differences in the kidney microbial signatures by gender identity (Two-way ANOVA f = 0.061, $p = 0.805$; Fig. 10b; Permanova f = 1.37, $p = 0.253$; Fig. 10c). Negative controls used in this analysis for decontamination were variable, but significantly different from positives, independent of source (Fig. 10d).

Scrutinization of microbiome data

To scrutinize and support the validity of the microbiome data generated from our analysis, we used a hybrid approach. First, we conducted statistical decontamination with Decontam, which removes 90% of contamination with minimal false negatives[53] and we also conducted a knowledge-based removal of common taxa found in laboratory reagents[54]. Statistical decontamination led to a 23% reduction in the number of unique taxa in the human data compared to a 19% when bacteria was censored through a knowledge-based approach. In mouse data, statistical decontamination led to a 2.3% reduction in unique taxa compared to a 35% reduction with the knowledge-based approach. It must be noted, however, that in mouse studies, multiple sources of negatives that were directly tied to the experimental procedures were used as negatives for statistical decontamination. Additionally, many of the taxa that have been identified as reagent contaminants[54] that we used for the knowledge-based scrutinization, such as *Enterobacter, Escherichia, Corynebacterium, Kocuria, Bacillus, Streptococcus*, and others, have been recurrently identified in the urinary tract microbiome[55]. As such, removal of these taxa would necessarily lead to a number of false negatives.

To assess the impact of decontamination methods on the statistical differences shown here, we compared the statistical significance in the beta diversity of human glomeruli vs. tubuli and mouse kidneys vs. urine. While the knowledge-based decontamination method led to a reduction in the statistical significance for both human and mouse data, beta diversity analyses were highly significant regardless of the decontamination method chosen (Fig. 11a, b). Additionally, to assess the impact of contamination on the statistical differences between groups, we simulated contamination in both the human and mouse data by using a random number generator to simulate universal, stochastically distributed taxa, similar to what would be seen with reagent-based contamination. In this analysis, we found that the number of contaminants exhibited a significant negative correlation with the beta diversity test statistic in both datasets (Pearson's correlation, r = -1, $p < 0.001$; Fig. 11c, Pearson's correlation, r = -96, $p < 0.001$; Fig. 11d).

Discussion

Recent studies have characterized the microbiome of intrarenal specimens, such as stones or kidney urine[7,17,56]. We hypothesized that the kidneys may harbor a low-density, antibiotic-sensitive microbiota that influences lithogenesis through microbial metabolic output. It has been recently suggested that to differentiate a microbiota with transient colonization, the former should exhibit: 1) Metabolic activity; 2) Stability over time; and 3) In situ replication[19]. Thus, to address our hypothesis, and having in mind these criteria, we conducted a comprehensive mouse study to quantify the distribution and antibiotic sensitivity of bacteria in kidney tissue. From rigorously controlled experiments, culture-based and imaging data show a viable and metabolically active kidney microbiota in all animals regardless of intervention (Fig. 1a–c), which was corroborated molecular data (Fig. 1d, f) and was consistent with human kidney microbial signal profiles (Fig. S9f,1e). Previous studies in SWJ/R mice show that transurethral inoculation of bacteria into the bladder leads to vesicoureteric reflux and pyelonephritis from inoculated bacteria[57–59]. In a diabetic mouse model, investigators found kidney bacteria due to gut translocation[60]. One other potential source of kidney bacteria is hematogenous spread[61]. In our study, there were clear differences between the kidneys and urine in mice (Fig. 1d), which suggests the bladder did not make a significant contribution to the kidney microbiome. In the present study, we conducted VUR phenotyping of male SWR mice[25], which reveals absence of this urinary tract defect, as further evidence that bacteria may not come from the bladder under

https://doi.org/10.1038/s41467-024-54432-6

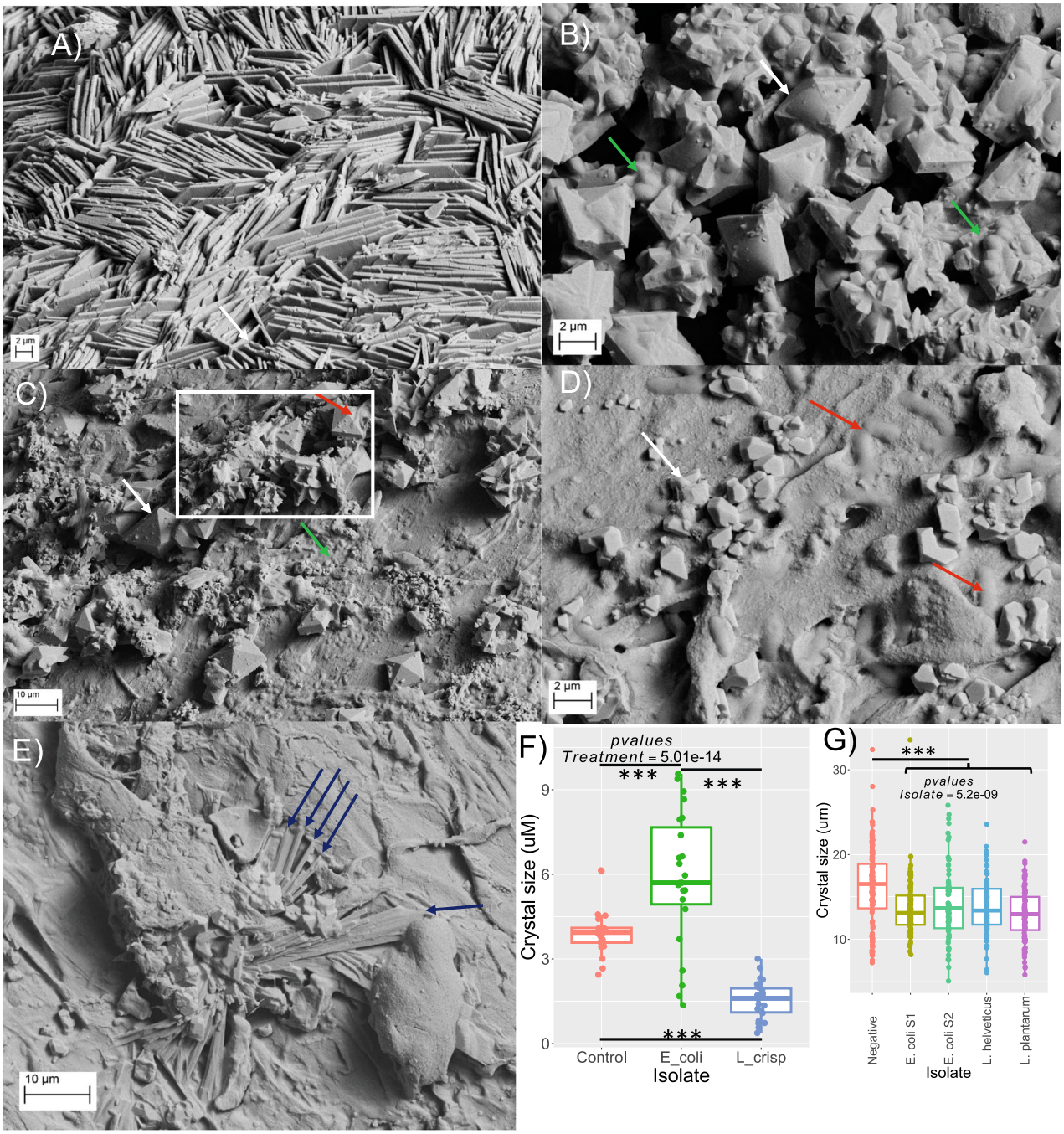

normal conditions. (Fig. 1h). Longitudinal analysis revealed a stable microbiome over 30-days (Fig. 3c). Collectively, our findings supports, the presence, metabolic activity, and stability of a renal microbiota in mice.

In human renal specimens, RNA-FISH analysis shows bacterial DNA, as a marker of microbial replication and viability, in 100% of the samples (Fig. 6). Importantly, RNAseq data, derived from human specimens and reanalyzed in the present study, came from polyA enriched RNA with oligo-dt beads, which seeks to eliminate microbial RNAs[52]. While this method reduces microbial signatures by 27-fold compared to conventional RNAseq, previous studies have shown that microbial signatures are not completely removed[62]. Given this, we estimate that the true proportion of microbial to host reads in nephrons is closer to 5% (based on Fig. 9a). The mRNA data derived from this study, as a marker of metabolically active microorganisms[63], was further evaluated to assess factors that shape these microbial signals. Microbial signatures were differentiated by proximity in the nephrons and was dependent on age and ethnicity, but not gender identity (Figs. S9, S10), consistent with a previous study[18]. Importantly, in both human and mouse data, we show that microbial signatures could not have resulted from either falsely annotating sequences as microbial (Fig. 9b) nor from contamination (Fig. 11).

While we did not investigate the potential origins of renal microbial signals, the age-based higher species richness in the glomeruli of humans compared to the tubules (Fig. 9c), sheds light on one potential source. Past studies have shown bacteria can translocate from gut to the kidneys with increased gut epithelial permeability[8], which is more notable in older adults[64]. There is a progressive loss of glomerular filtration with age, in part due to an age-related loss of glomeruli[65]. Our data suggest that the potential loss of the glomerular

Fig. 4 | SEM images of in vivo and in vitro CaOx crystals. A Surgically removed CaOx kidney stone exhibiting laminated sheets of mineralized CaOx. **B** CaOx crystals formed in the absence of bacteria, through non-canonical processes whereby nano-sized CaOx spheres (green arrows) aggregate to amorphous forms and eventually to the classical octahedral, dihydrate structure (white arrows). **C** CaOx crystals formed in the presence of *E. coli*, through non-canonical pathways. Bacteria (red arrows) were seen growing on CaOx crystals. White box encloses a large CaOx crystal aggregate. **D** CaOx crystals formed in the presence of *L. crispatus*. Crystals that formed (white arrows) were either arrested at the amorphous phase or were broken down by microbial processes. Bacteria (red arrows) did not grow on crystals. **E** CaOx crystals formed in the presence of both *E. coli* and *L. crispatus*. Crystalline structures (blue arrows) are indicative of CaOx monohydrate, indicative of a shift in chemistry when bacteria were co-cultured. **F**, **G** Quantification of CaOx dihydrate crystal size in each microbial condition in bioreactor assays (**F**; N = 21-26/group; df = 67; control:E_coli −t = 4.09; p = 0.00012; control:L_crisp − t = 5.49; $p = 1.3 \times 10\text{-}6$; E_coli:L_crisp − t = 9.95, $p = 2.3 \times 10^{-14}$) and plate-based assays (**G**; N = 78-135; df = 488; t = 3.87-6.18 for significant values; $p = 1.3 \times 10^{-8}$-0.00086 for significant values). ANOVA results are shown with post-hoc paired, Holm's-corrected t-tests. ** p-value < 0.01; *** p-value < 0.001. For box and whisker plots; the center is the data mean, minima and maxima are the 25th and 75th percentiles; whiskers extend 1.5 interquartile range from minima and maxima. Source data are provided as a Source Data file.

basement membrane integrity due to the progressive decrease in kidney clearance with age, may allow some bacteria to pass from the blood into the glomerulus. With the loss of glomeruli, red blood cells, which are up to eight times larger than individual bacteria, can infiltrate the urinary space[66] and may also allow for the colonization of bacteria. Given the limitations with the human data, we could not establish stability. However, image-based and molecular data provides evidence for the presence of a viable and metabolically active microbial signals in humans. In all kidney specimens, microbial signals were evident in the glomeruli and tubuli, with clear differences in microbial density and composition, consistent with similar analysis[18]. Causative implications of these findings for disease remain to be determined. It's important to note that while mice had a higher bacterial density in the more distal region of the kidneys (Fig. 1b), there was greater density apparent in the proximal end of the kidneys in humans (Fig. 9a). Given that the mice strain used in this study was negative for VUR phenotype (Fig. 1h), the most likely explanation for this discrepancy is the positive correlation of increasing age and increased species diversity in the glomeruli but not the tubuli in humans (Fig. 9c).

Cefazolin is a common antibiotic prophylaxis in surgical procedures that can cause gut dysbiosis and colitis[67], is associated with future risk of nephrolithiasis[68], and is excreted unchanged in urine[69]. In mice, seven days of cefazolin exposure significantly impacted the urobiome (Figs. 2a, b, S4a, b). In the present study, taxa previously associated with lithogenesis and infection, such as *Enterococcus* and Enterobacteriaceae[15,70], were not impacted by long-term antibiotics (Figs. 2d, e, 3d–f). Conversely, uroprotective lactic acid strains like *Lactobacillus* and *Lactococcus*[7,71,72], were significantly disturbed (Figs. 2d, e, 3d–f). Past research shows that antibiotic use can promote translocation of colonic bacteria[73], which could potentially lead to the transient presence of bacteria in the circulation and in the kidneys. Our data show that antibiotics induced a species-specific decline in abundance (Fig. 3d, f), indicative of a microbiota responding to an environmental perturbance, rather than translocation. Overall, results show that cefazolin can drive a dysbiosis in the murine kidney microbiota towards antibiotic-resistant uropathogens.

Urine supersaturation with crystallizing salts has been associated with the development of a renal inflammatory response and interstitial crystal deposition[35], as has urinary dysbiosis and the proliferation of uropathogenic bacteria, such as *E. coli*[15,17,74,75]. In the present study, cefazolin and urinary dysbiosis was associated with an increase in pro-inflammatory cytokines (Fig. 2f), which could result from antibiotic exposure directly, or from differential exposure to dietary or microbial elements, and suggests that disturbance of the urinary microbiome can cause changes in the urinary environment that can trigger immune responses in the kidney and enhance lithogenic steps like tubular cell-crystal adhesion[32] that warrants further investigation.

While studies have illuminated the beneficial and pathogenic impacts of *Lactobacillus* and *E. coli*, respectively for urologic health[7,8,74], questions remain about mechanisms driving this phenomenon. Our study points to antibiotic resistance by Enterobacteriaceae as one means of dysbiosis, but we also observed occasional outbreaks by Enterobacteriaceae in addition to direct competition between Enterobacteriaceae and *Lactobacillus* (Figs. 3g, S6b, c), consistent with previous studies[76]. We observed that a specific strain of *E. coli* (ATCC 43886) out-compete *L. crispatus* (Fig. S7a–c) through bioreactor studies, consistent with genomic analysis (Fig. 6a), but is in contrast to previous findings of adhesion inhibition of *E. coli* by *Lactobacillus* strains[11].

Past studies have shown that *E. coli* enhances the growth of CaOx cyrstals[15,77]. Our bioreactor studies show that this effect can be modified by the presence of other bacteria such as *L. crispatus*. When grown alone, a specific strain of *E. coli* promoted and *L. crispatus* inhibited development of CaOx crystals through a known non-canonical pathway whereby nano-sized droplets aggregate to first form amorphous crystals, that further aggregate into octahedral shapes and then more complex structures (Fig. 4)[43]. While *E. coli* attached to and facilitated the growth and aggregation of crystals, *L. crispatus* did not attach to crystals and halted lithogenesis at the amorphous stage, similar to known inhibitors (Fig. 4)[78,79]. The differential impact of these species on crystal growth could be due to the production or degradation of oxalate, respectively (Fig. 7e). However, EDS analysis revealed significantly different elementomes in crystals that developed under different microbial inocula (Figs. 5, S8). Specifically, *L. crispatus* produced crystals enriched in sulfur, a known calcium competitor[47,48] and phosphorus, another calcium competitor linked to urolithiasis inhibition[44–46]. *E. coli* produced crystals enriched in iron and chloride, which are both known CaOx crystal promoters and are common elements in biofilms[44,49–51]. When *E. coli* and *L. crispatus* were co-cultured, crystal morphology switched from octahedral to styloid (Fig. 4). Common uropathogens, like *Klebsiella pneumoniae* and *E. coli*, have also been shown to enhance CaOx crystal growth and aggregation in vitro[77] through bacterial proteins and the net charge of crystal ions[15]. *E. coli* was found on both dihydrate and monohydrate forms of crystals (Fig. 4). This finding corroborates *E. coli* attachment to abiotic and CaOx surfaces[17,79]. Collectively, we provide evidence that pro-lithogenic and anti-lithogenic microbe dynamics influence a diverse range of steps in the development of CaOx stones, from the availability of crystallizing salts to the development of crystal polymorphism. Importantly, the effect of these empirically chosen *E. coli* and *Lactobacillus* strains do not necessarily extend to related taxa. In other species of lactic-acid bacteria and additional strains of stone-derived *E. coli*, we found that while all isolates influenced CaOx crystal size, these new strains universally decreased crystal size, which suggests that the *E. coli* strain used in the bioreactor studies, which is the most abundant found across multiple stone types, exerts its influence in strain-specific ways, while lactic-acid bacteria may exhibit a more common mechanism to inhibit crystal growth. Previous studies have suggested that net electrostatic potential on the surface of bacterial appendages like flagellum can interact with the surface of CaOx crystal[15]. This protein distribution, on bacterial surface, can potentially vary by different strains of the same bacteria and determine whether CaOx growth is promoted or inhibited[80].

In conclusion, the data of the present study, derived from multiple, independent approaches show that a low biomass microbial community may be present in microniches of kidneys from humans

https://doi.org/10.1038/s41467-024-54432-6

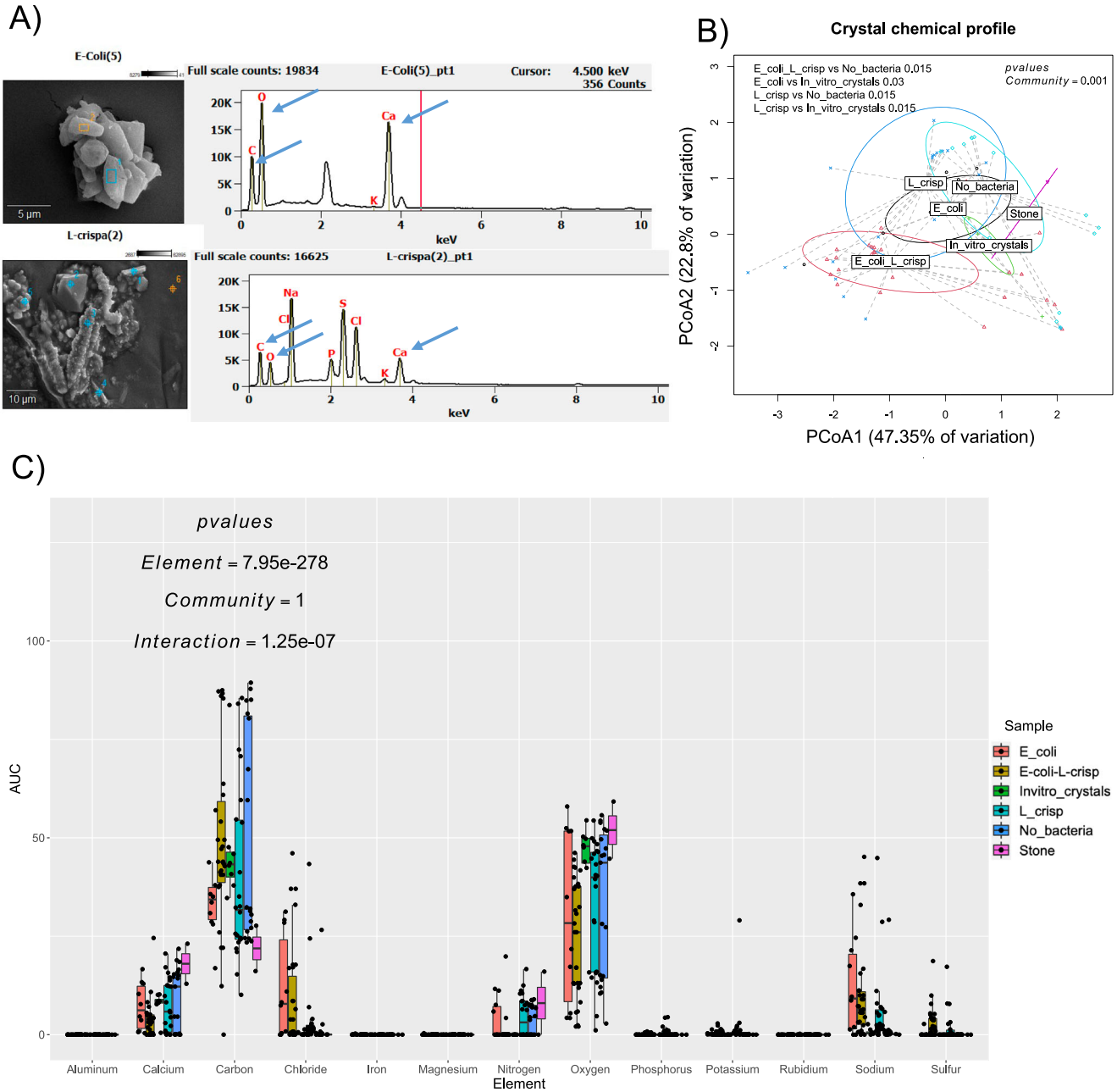

Fig. 5 | X-ray diffraction (EDS) of CaOx crystal formation in vivo or in vitro. **A** Representative EDS chromatograms from *E. coli* (top) and *L. crispatus* (bottom), with peaks for CaOx highlighted (blue arrows). **B** PCoA representing the elemental analysis of CaOx crystals in each of the treatments. Statistical comparision was based on PERMANOVA (1-way global and 2-way, Holm's corrected analyses) on the binomial distribution of elemental profiles (N = 10-30; for surgical stones $N = 2$; df=90; f = 4.8534; $p = 0.001$. **C** Comparison of the area under the curve for each element detected in crystals. Statistical analysis was a 2-way ANOVA ($N = 10$-30, except for kidney stones; df = 90 f = 0 for community, 17557 for element, and 2.319 for interaction; $p = 1, 2 \times 10^{-16}, 1 \times 10^{-7}$, respectively. Targeted analyses of all elements that show significant treatment effects are presented in Fig. 8. For box and whisker plots; the center is the data mean, minima and maxima are the 25th and 75th percentiles; whiskers extend 1.5 interquartile range from minima and maxima. Source data are provided as a Source Data file.

and mice. This community is perturbed by antibiotics, generating a pattern of dysbiosis which suppresses *Lactobacillus*, and proliferates Enterobacteriaceae. *Lactobacillus* and a specific strain of *E. coli* may modified the chemical environment to influence CaOx lithogenesis. Collectively, data suggest that the association between antibiotic use and the onset of urolithiasis can be driven, in part by a loss of *Lactobacillus* in the kidneys, which allows antibiotic resistant Enterobacteriaceae to proliferate. This may lead to a change in the local chemical environment to facilitate CaOx lithogenesis through the potential production of CaOx promoters, which would be an independent risk factor to other known biochemical risk factors for stones[32]. Collectively, our animal experiment suggests that conventional antibiotics may shift the kidney microbiome towards more pathogenic/lithogenic bacteria. As such, to help prevent lithogenesis, good antibiotic stewardship combined with the development of alternative or more targeted bacteriotherapies are needed, such as quorum-sensing inhibitors that target biofilm formation or urinary *Lactobacillus* probiotics that can restore uroprotective bacteria to the urinary tract.

We acknowledge the limitations of the study. First, evidence of the human bacterial signature is limited to molecular and imaging data, with human molecular data not collected specifically for microbiome

https://doi.org/10.1038/s41467-024-54432-6

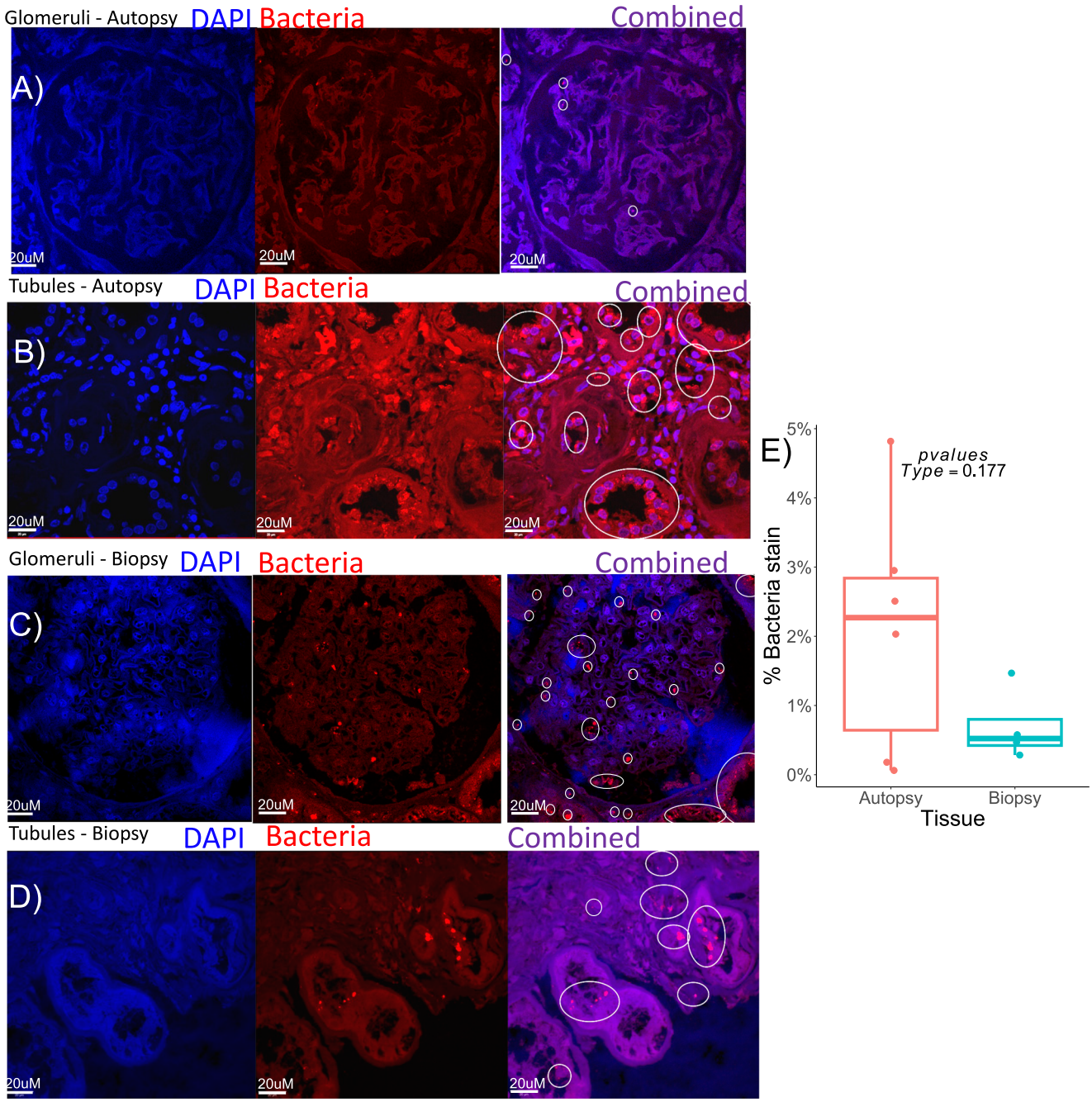

Fig. 6 | RNA-FISH imaging of in situ bacteria in human kidney tissue. A universal bacterial FISH probe (red) with nuclear DNA detected with DAPI (blue) in kidney tissues obtained either in autopsy (**A**, **B**) or as biopsy (**C**, **D**). Bacteria was detected in glomeruli (**A**, **C**) and in the tubulointerstitium (**B**, **D**). For each image, the individual DAPI and bacteria channels are shown, along with the combined channel overlay. Bacterial signals indicated by fluorescent red, circled in white in the combined images. **E** Statistical comparison of the area of bacterial stain relative to total kidney tissue area between biopsies and autopsies. Statistical comparison was a t-test. Representative images were taken from $N = 6$ for autopsies and $N = 4$ for biopsies. df=9, t = 2.195, $p = 0.177$. All data is shown in Fig. 6E. For box and whisker plots; the center is the data mean, minima and maxima are the 25th and 75th percentiles; whiskers extend 1.5 interquartile range from minima and maxima. Source data are provided as a Source Data file.

analyses. Additionally, our mouse study was designed to assess the baseline murine kidney microbiome, and tests of hypotheses for the influence of urinary tract bacteria and lithogenesis were done in vitro. Importantly, to eliminate sex-based anatomical biases, studies were only done in male mice. Given these limitations, follow-up in vivo studies are needed in germ-free mice with an appropriate stone-forming rodent model, which includes both male and female mice. Finally, we note that DESeq2, the differential abundance algorithm used here, can be limited in microbiome studies[81]. However, ANCOM analysis produced similar results in our study (Fig. S9g,h).

Methods

The present research complies with all relevant ethical regulations

All animal procedures were approved by the Institutional Animal Care & Use Committee of the Lerner Research Institute (IACUC # 2020-2312)

and performed in accordance with institutional guidelines. Human kidney samples were obtained through the pathology department at the Cleveland Clinic (IRB# 20-847) from kidney biopsies and from tissue harvested from autopsies, in which family consent was given for tissue collection for submission to the local biobank for research purposes (IRB# 20-403). Study approval and a consent waiver were obtained from the Cleveland Clinic to use archival formalin-fixed paraffin blocked kidney tissue considered discard from with less than minimal risk to subjects. Tissue was provided without patient identifiers and no protected health information was collected. Publicly available data from human kidney samples deposited in the sequence read archive (BioProject PRJNA725213) were reanalyzed in the present study to investigate the presence of microbial signals.

Low microbial biomass considerations. Recent research has focused on the presence of a low biomass microbiome in entrapped organs previously thought to be sterile[19,82]. Where possible, recommendations put forth for the study of low biomass microbial communities and the discovery of a microbiome were followed in the current study to prevent, assess, and eliminate contamination[19,82]. For this purpose, we followed the suggestions of RIDE guidelines through the inclusion of multiple negative controls, bioinformatic decontamination, and reporting contaminants for animal studies. Molecular human data were limited in that no internal negative controls were available. To overcome this limitation, we conducted a hybrid approach with the use of: external negative controls from two clinical microbiome studies of the urinary tract from two different sites as discussed below, and a knowledge-based approach with the removal of taxa previously described as reagent contaminants[54]. For the discovery of a microbiome in the kidneys, we followed the recommendations of an expert panel, in which a microbiome must be 1) metabolically active; 2) reproduce in situ; and 3) is stable over time[19].

Animal studies. To eliminate sex-based biases associated with LUT anatomy, one-hundred sixty 3-week-old SWR/J male mice[83] (RRID:IMSR_JAX:000689) were purchased from The Jackson Laboratory and maintained at the Cleveland Clinic Biological Resources Unit. All mice were housed four to a cage in metabolic cages, with a 12-h/12-h light/dark cycle, at 28 °C and 20% humidity. After 5-days acclimation and through the duration of the diet trial (Fig. 1a), mice were fed with a 1.5% oxalate pelleted diet (Supplementary data 6), adjusted with $Na_2C_2O_4$ (Fisher Scientific, Pittsburgh, PA) on a dry weight basis. At four weeks age, animals were randomized into eight treatment groups, four cages per group for a total of 16 animals in each intervention or control arm. Four groups of mice received antibiotic-free water and four received cefazolin sodium salt, 98% (Fisher Scientific) in water (0.125 g/L) for either 3 days (short-term) or 14 days (long-term) (Fig. 1a). During antibiotic exposure, all animals received water with 2 g/L sucralose. This concentration and duration of cefazolin elicits a significant drop in gut microbiota diversity and microbial oxalate metabolism in SWR/J mice[34]. Throughout the post-acclimatization phase of the diet trial, urine was collected daily in sterile collecting funnels and pooled in three-day intervals for microbial analyses. To help prevent contamination from the stool or fur, the collecting cones of the metabolic cages were disinfected daily, new sterile collection funnels were placed daily, and any urine specimens with fecal pellets were discarded. Urine samples were frozen at −20 °C for less than 6 months prior to DNA extraction. After three or fourteen days of intervention, half of the animals from the short-term and long-term arms were necropsied. The remaining animals were allowed to recover for 14 days and given antibiotic-free water *ad libitum* prior to necropsies (Fig. 1a). Necropsies were conducted in a disinfected biosafety cabinet with sterile gloves and instruments. Animals were disinfected with 70% ethanol, and kidneys were aseptically collected[84] and rinsed with sterile saline. One kidney from each animal was frozen in sterile PBS at −20 °C, prior to DNA extraction. The remaining kidney was fixed in 10% formalin overnight and stored at 4 °C in 70% ethanol to prevent environmental contamination[38], prior to histological processing. Vesicoureteral reflux testing in SWR/J male mice

To exclude the presence of bacteria coming from a potential vesicourteral reflux (VUR) in our experimentation animals, 5 SWR/J male mice at 12 weeks of age were phenotype for this urinary tract defect. Briefly, animals were euthanized, made hypothermic on a pietri dish with ice, and surgically manipulated under microscope magnification to remove tissue and organs covering the urinary tract. The bladder was puncture with a 26-gauge 3/8 needle connected to a system of an IV tubing and a 60 ml syringe filled with 70% methylene blue. The syringe was raised vertically from 30 to 150 cm by 30/5 seconds intervals and maintaining it for 10 seconds once the final height was reached. The height of the column was record if there was any passing of dye to any of the ureters, individually assess under microscope, or escape through the urethra[25].

Calcium oxalate lithogenesis model. For in vitro assessment of bacterial influences on CaOx mineralization, a CDC Biofilm Reactor (BioSurface Technologies Corp.) was used (Fig. 1b). This system is a specialized continuous flow stirred tank reactor chemostat model that has been used to model the urobiome and lithogenesis[40]. It enables control of biofilm-related activity in a physical and chemical environment that mimics the urinary tract, in part through the use of AUM (Supplementary data S4)[85]. The original AUM recipe was amended with 5 g/L of meat extract (OXOID) to facilitate growth of *L. crispatus*. The system consists of a media reservoir, a chemostat with a stirring vane and eight suspended coupon holders, with eight polycarbonate coupons each (RD128-PC), that provide a substrate for biofilm attachment and growth, and a waste reservoir. The chemostat is placed on a stir/hot plate with a pump to transfer media from the reservoir to the chemostat at a constant flow rate. The AUM and control of the physical parameters of the bioreactor were designed to mimic the flow rate, temperature, chemical environment, and shear forces in the kidneys[40].

Specific strains of *L. crispatus* and *E. coli* used for lithogenic assays were chosen based on a previous clinical microbiome study of the urinary tract from patients with or without kidney stones[7]. The identity *L. crispatus* was verified through shotgun metagenomics[9] and the specific strain of *E. coli* through ASV[70] and phylogenetic analyses. Representative isolates were purchased from ATCC (ATCC 33197 and ATCC 43886) and verified through sequencing of the full length *16S rRNA* gene with 27 F and 1492 R primers. For every experiment, 3 liters of AUM was prepared and filter sterilized. Filter-sterilized solutions of calcium chloride (Fisher) and sodium oxalate (Fisher) in Milliq water were added to media at a concentration of 1 mMol. Then, 350 ml of media was placed in the chemostat and the rest in the system reservoir. Subsequently, AUM was pumped to the chemostat at a rate of 1 ml/min and stirred at a rate of 150 rpm at 37 °C. Prior to inoculation, bacteria were acclimated in static AUM for 72hrs, washed 3 times by centrifugation at 4,500 x g and resuspended in sterile PBS before being diluted to an optical density at 600 nm of 0.4. 100µl of bacteria or sterile AUM was inoculated for bioreactor assays with the following treatment groups: 1) Sterile media alone (negative control); 2) *E. coli* alone; 3) *L. crispatus* alone; and 4) A combination of *E. coli* and *L. crispatus*. AUM flow was started immediately after inoculation and continued for 72 hours. After incubation, coupons were removed from holders to assess mineral accumulation and an aliquot of the bioreactor media was sampled to quantify the viability and abundance of each taxa within the media (discussed below).

Bacterial viability assay from bioreactor experiments. The proportion of live bacteria in bioreactor effluent was analyzed using the LIVE/DEAD BacLight Bacterial Viability Kit (Molecular Probes, Invitrogen; L7012). Fresh bacterial suspensions of *E. coli* and *L. crispatus* with

known proportions of viable and non-viable bacteria were used to create a standard curve of viable cells. Assays and analyses for each sample was performed following the manufacture's protocol Control samples, and aliquots of the media from the bioreactor were analyzed using fluorescent spectroscopy.

qRT-PCR. To quantify the abundance of each taxa from the bioreactor experiments, *E. coli* and *L. crispatus* were detected and quantified using qRT-PCR as described[86] using a universal bacterial primer as a standard[87,88]. Bioinformatic analysis of genomes was used to design species-specific primers for *L. crispatus* and *E. coli* (Supplementary data S7). Extracted DNA from each strain was used to validate primer specificity prior to qRT-PCR quantitation. Efficiency of each primer set was above 90%.

Mineralogical analysis of the coupons. Field emission-SEM (FE-SEM) was used to quantify minerals attached to air-dried coupons. A clinically- extracted, pure-CaOx stone and in vitro CaOx crystals were included as positive controls. For FE-SEM a Zeiss Sigma VP scanning electron microscope was used, at a voltage of 5 – 10 kV and resolution between 2 and 10 nm. Crystal size was quantified in ImageJ. FE-SEM and energy dispersive x-ray spectroscopy (EDS) was done to observe mineral shapes and quantify near surface chemistry. For EDS, coupons were pressed to a SEM sample mount covered with carbon tape, leaving solid material attached to the tape. Samples were sputter coated with 5 nm of gold in a EMS150T ES Sputter Coater and imaged with Zeiss Sigma EM coupled with an UltraDry Xray spectroscopy detector for elemental analysis.

CaOx crystallization assays on representative bacteria strains. To analyze the influence on dynamics of crystallization from additional strains of *E coli* and lactic-acid bacteria, plate based crystallization assays were conducted. From a stored biobank of bacteria, 2 other strains of E coli, isolated from CaOx stones, and identified through sequencing, and 2 strains of lactic-acid bacteria (*Lactiplantibacillus plantarum* and *L. helveticus*) purchased from ATCC were enriched in BHI broth for 48 hours. CaOx crystallization assays were performed through a modified protocol. Briefly, aliquots from each enriched bacteria were washed 3 times and resuspended in PBS before being dilutes at 600 nm of 0.4. Then, 10 µl of the resuspended bacteria were added into Nunc Glass Base Dish (Thermo Scientific), containing 2 ml of 10 mM $CaCl_2$ in a basic buffer (10 mM Tris HCL and 90 mM NaCl, ph 7.4). Thereafter, 2 ml of 1 mM $Na_2C_2O_4$ in the basic buffer was added and incubated at 25 °C for 60 min. Crystal images were captured randomly from 4 power fields under Leica DMi1 inverted microscope at 40X. Crystal size and number were quantitated using ImageJ software in triplictes from each experiment. An assay without bacteria was also run as a negative control for comparison[15].

Genomic analysis and in vitro validation of study results. Genomic analysis was performed on *L. crispatus* and stone-associated *E. coli*, followed by additional in vitro assays for oxalate metabolism and antibiotic resistance. Genomes associated with ATCC strains were downloaded from ATCC and full-length genes extracted and annotated with PROKKA[89]. Subsequently, genes associated with lithogenesis, antibiotic resistance, biofilm formation, or oxalate metabolism were quantified. To validate the impact of antibiotics on *Lactobacillus* and Enterobacteriaceae, pure cultures of *L. crispatus* and the stone-associated *E. coli* were plated in triplicate on MRS (Oxoid) or MacKonkey agar (Oxoid), respectively, along with paper disks (Oxoid) containing ampicillin, cloranfenicol, penicillin, or tetracycline. After 48hrs incubation, the zone of inhibition was quantified. To validate the interaction between *L. crispatus* and the stone-associated *E. coli* with oxalate, bacteria were grown in broth culture (MRS for *L. crispatus* and BHI for *E. coli*) that contained 5 mM of $Na_2C_2O_4$ as preliminary studies indicated that greater oxalate concentrations inhibited the growth of *L. crispatus*. The supernatant of the broth culture was assayed for oxalate content using a potassium permanganate titration assay following oxalate extraction[90] at 0, 3, 5, 14, and 21 days after inoculation. Sterile media was used as a negative control.

Histopathology and FISH-based bacterial quantification. To quantify the presence of bacteria in mice kidney tissue at the domain, family or genus level, three RNA-targeted FISH probes were purchased (Invitrogen). Probes included a universal probe that targets all bacterial taxa (EUB388; GCTGCCTCCCGTAGGAGT)[91], an *Enterobacteriaceae*-targeted probe (pB-00914; CTCTTTGGTCTTGCGACG)[92], and a *Lactobacillus*-targeted probe (gC-358a; CCATTGTGGAAGATTCCCT)[93]. A 5µM stock solution of each probe was prepared in sterile Milliq water and stored at −20 °C[94].

Formalin-fixed kidneys were longitudinally bisected, paraffin embedded, and sectioned after disinfecting equipment. Blocks were sectioned (3 µm thick) on a rotary microtome (Medim, Type DDM 0036). Fixed suspensions of *Lactobacillus sp.* and *Enterobacter sp.* isolates obtained from murine urine, were used as positive controls to validate probe specificity. Slides with no bacteria as negative controls were assessed to determine the presence of contamination in reagents. In addition, to assess the presence of false positives generated by autofluorescence or non-specific binding, each probe was randomly scrambled and a set of samples were stained in parallel with either the targeted or the untargeted probe, as previously described[95]. To stain slides with FISH probes, serial tissue sections were incubated at 60 °C for 1 hour and immersed in xylene, ethanol and MilliQ water. The FISH probes (50 µl/slide) were prepared by mixing 1 part of the probe, 1 part of hybridization buffer (100 mM of Tris–HCl (pH 7.2), 0.9 M of NaCl, and 0.1% of SDS), and 1 part of RNA stabilization solution[94]. Bacterial suspensions and deparaffinized tissue sections in triplicate were stained with DAPI and either one of the three FISH probes. A cover slip was placed on the stained tissue and incubated on a heating block for 90 minutes and washed with a washing buffer (100 mM of Tris-HCL (pH 7.2), 0.9 M NaCl, 0.1 mM SDS) for 30 minutes. Finally, 50 µl of VECTASHIELD antifade mounting media (Fisher Scientific, nc9029229) was added to dry slides and stored 24 hours at 4 °C. Slides were scanned with an Artemis confocal microscope with channels for each of the fluorescent probes. After the specificity and immunofluorescence thresholds of the probes were established with pure cultures of *Lactobacillus* and *Enterobacter*, stained kidney tissue was analyzed to enumerate bacteria. Bacterial counts were averaged for each slide and normalized to the surface area of the kidney section (bacteria/cm^2 of kidney tissue). A Holm's-corrected paired t-test was used to statistically compare bacterial counts between treatment groups.

Four clinical biopsy and six autopsy specimens were acquired through the pathology department at the Cleveland Clinic to validate the presence of bacteria in human kidney tissue. Specimens were collected from May 2020 to February 2022 from in-patients undergoing punch kidney biopsies in the course of routine care for diagnostic purposes and from tissue harvested from autopsies. The kidney samples were processed by the clinical pathology department using their standard fixation procedure in formalin. The residual paraffin blocks from biopsies and autopsies were archived within the institutional pathology department. No clinical data, as well as age or sex, were considered for this analysis. Since bacteria in human tissue were often present in overlapping clusters, stained bacterial area, rather than individual bacteria, were quantified relative to total tissue area. For histographs in Fig. 6, brightness and contrast were uniformly altered to make the fluorescent staining more apparent. Quantification occurred in QuPath targeting the fluorescent stain. To assess the presence of contaminants, we analyzed all borders of the tissue section and the surroundings for the presence of randomly distributed

bacteria, which is a sign of contamination, as previously described[38]. As an additional control for autofluorescence and non-specific binding in the tissue from mice, all FISH stained kidney sections were assessed with four fluorescent channels pertaining to DAPI and each of our three microbial probes. If signals were present in multiple channels, they were not counted. Additionally, serial mouse tissue sections were stained with three unique microbial probes that target all, *Lactobacillus*, or Enterobacteriaceae taxa. If signals were present using multiple probes, indicative of autofluorescence, they were not counted.

Culture-based bacterial quantification in urine and kidney tissue. The presence of a murine kidney microbiota was validated through culture-based means whereby three, 10-week-old mice in a clean barrier facility were necropsied and the kidneys aseptically excised and longitudinally bisected. A sterile inoculation stick, 1 mm in diameter, was inserted 1 mm into either the cortex, medulla, or ureter. Sticks were used to streak culture plates (Fisher Scientific) containing Columbia blood agar, CNA blood agar, chocolate agar, and brain heart infusion agar, in triplicate. Negative controls included sterile sticks without kidney insertion. Plates were incubated aerobically for 72 hrs before quantifying CFUs.

To quantify the abundance of Enterobacteriaceae and *Lactobacillus* in urine at each timepoint, serially diluted urine was plated aerobically on MacConkey (Oxoid) or MRS agar (Fisher Scientific), respectively, and incubated for 48 hours at 37 °C prior to counting of colony-forming units (CFUs). Data were compared with a two-way ANOVA followed by post-hoc, Holm's-corrected, paired t-tests.

Quantification of urinary cytokine levels. Concentrations of IL-6 (R&D Systems), IL-18 (Fisher Scientific), and IL-1β (R&D Systems) were quantified with ELISA-based assays, following the manufacturer's instructions. Positive controls of a known amount of substrate and no substrate-negative controls were included in all batches. Samples, standards, and controls were run in duplicate and values averaged by sample. Due to limitations of urine volume, we prioritized microbiome analyses and could not perform other biochemical assays, such as urinary oxalate. We previously reported the impact of cefazolin on urinary oxalate in this animal model[34].

Metagenomics and bioinformatic analysis. For DNA extraction, mouse urine was centrifuged at a 3000 x *g* for 5 minutes and the pellet was used for subsequent processing or kidney tissue was aseptically morcellated in a sterile mortar and pestle in 1 ml of sterile PBS and vigorously vortexed until a homogenized solution was achieved. The suspension was then processed with a MolYsis Basic 5 Kit (MolYsis Life Science, Bremen, Germany) to lyse residual animal cells and remove host DNA[96]. Either 400µl of pelleted urine or homogenized kidney tissue was used for semi-automated DNA extraction on a KingFisher Duo Prime system (Thermo Scientific) following manufacturer's instructions. From extracted DNA, the *16S rRNA* gene was amplified with the 27 F and 1492 R universal bacterial primers for a subset of urine and kidney samples to validate the presence of bacterial DNA prior to high-throughput *16S rRNA* sequencing. For high-throughput *16S rRNA* sequencing, extracted DNA was submitted to the Microbial Sequencing & Analytics Facility at the Lerner Research Institute (Cleveland, OH) for 150 bp, paired-end sequencing of the V4 region of the *16S rRNA* gene, with primers 515 F and 806 R on an Illumina MiSeq[97]. Duplicate samples of a commercial DNA positive (Zymobiomics, USA) were run with each sequencing plate to determine if the sequencing run itself impacted community composition. Negative controls that included sterile PBS, mouse chow, antibiotic-free water, and water with cefazolin were run in tandem with the urine and kidney samples through the entire workflow for animal studies. We also included sampling blanks, DNA extraction blanks, and no-template amplification blanks in each batch, following suggestions from RIDE guidelines for low biomass studies[82]. Contaminants from the mouse study were identified with decontam and represented 43 out of 1852 ASV's identified (Supplementary data S8). For mouse data, negative controls presented a direct potential source of contamination.

To investigate the presence of microbial signals in human kidneys, the sequence read archive was searched for data derived from shotgun metagenomics, transcriptomics, or *16S rRNA* sequencing, and originating from human kidney tissue. Only one study fit the criteria (BioProject PRJNA725213), which included RNA-seq data from laser microdissected glomeruli and tubuli of humans[52]. From this study, we used a batch that only included healthy individuals. Raw sequencing data was screened for adapter sequences and sequences with a Phred score <20 with bbduk[98]. High-quality data was then mapped to the GRCh38 human genome to remove host reads, with BWA mem[99]. For publicly available human data, which was not designed as a microbiome study, external positive and negative controls from other clinical urobiome studies from two different sites (San Diego, CA and Cleveland, OH; unpublished data) were assessed, as well as the removal of potential contaminant taxa[54] through a knowledge-based approach to eliminate taxa typically associated with plants or extreme environments (Fig. 10d). Use of the external negative controls and a knowledge-based approach led to a conservative approach for contaminant removal and 751 out of 3186 taxa were removed (Supplementary data S9).

All bioinformatic analyses were conducted in R statistical software[100], unless otherwise noted. Quality control, chimera removal, and assignment of amplicon sequence variants (ASV) were completed in dada2[101]. For ASV assignment, a dereplicated database containing *16S rRNA* sequences from the Silva 138 SSURef[102] and NCBI *16S rRNA* databases[103] were used for mouse data while a database of 30,052 full-length Prokaryotic genomes downloaded from the NCBI were used for non-host RNAseq data derived from human kidney samples. Taxa assigned to mitochondria, Eukaryotes, or chloroplasts were removed from all samples prior to subsequent analysis. For all datasets, threshold sequencing depths needed to adequately reflect community diversity per sample were calculated through rarefaction analysis in vegan[104], which we defined as the sequencing depth at which >90% of samples had a slope of <0.01 in the rarefaction analysis. For *16S rRNA* data, ASV's were aligned in MSA[105] and arranged into a maximum likelihood phylogeny in phangorn to produce a phylogenetic tree.

The raw count tables from human or mouse sequencing data were normalized to the number of host reads. From the normalized count tables, we calculated the following α-diversity metrics: species richness (Margalef's), evenness (equitability), Shannon index, and phylogenetic diversity (*16S rRNA* data only). We analyzed diversity metrics with a repeated-measure ANOVA and *post hoc* Tukey's analysis or a paired t-test with Holm's correction where applicable, after testing for data normality. A weighted UniFrac analysis (*16S rRNA* data) or weighted Bray-Curtis analysis (human data) was performed to compare community composition. Comparisons between treatment groups and timepoints were made with a 2-way PERMANOVA after 999 permutations.

To assess the potential impact of contamination on microbial data, we simulated universal, stochastically distributed contamination in mouse and human datasets using a random number generator, assigning values ranging from 0-100 in each of the samples. Simulated contaminants were added onto data that had already been decontaminated with Decontam, which is what our initial results were based on (Fig. 1d, S9e). Unique datasets were generated that contained simulated contaminants from 0-150 for both mouse and human data. Subsequently, the beta diversity test statistic was calculated for each dataset, comparing the glomeruli and tubuli (human data) or kidney and urine (mouse data) and a Pearson correlation was used to assess the correlation between the number of contaminants and differences in microbiome compositions.

Statistics and reproducibility. The animal study was designed with 8 groups based on short or long term antibiotic intervention with or without 14 days recovery, as well as control counterparts. Each group was represented by 4 cages of 4 animals each. After the acclimation period the animals were randomly allocated in each group. Assessment of bacterial viability, qRT-PCR, mineralogical analysis of the bioreactor coupons, CaOx crystallization assay of representative bacteria were conducted in triplicate. Replicate numbers are specified for each condition and were determined by conducting a power analysis in the *pwr* package in R, with a power of 0.8 and a medium effect size for all experiments, based on results from similar animal and clinical studies conducted in the lab previously. Clinical data was excluded from the human FISH analysis. The FISH data from murine kidneys was blinded and quantified by two independent reviewers. Quantification from the two reviewers were averaged prior to analysis.

All values, representing individual samples, are shown for boxplots, PCoA plots, and correlations. Bar and line graphs display mean values + /-SE. Differentially abundant ASVs (FDR < 0.05) are grouped by lowest assigned taxonomy and plotted as number of ASVs/taxon. Statistical analyses included ANOVA, after testing for data normality, and Holm's corrected paired t-tests, Pearson correlation with significant correlations based on the Pearson product-moment correlation coefficient, PERMANOVA with 999 permutations, based on either a weighted UniFrac or Bray Curtis dissimilarity matrices. Differential abundance analysis was based on the DESeq2 algorithm, which calculates the $\log_2$ fold difference +/-SE of DESeq2 normalized counts, between groups[106]. While other differential abundance algorithms have been developed for microbiome-specific data, such as ANCOM-BC[107], these algorithms are prone to type I and II error if groups are highly divergent (i.e. comparing different tissue types), and if the sample size is >10 between similar comparative groups, results and type I, II errors are comparable between DESeq2 and ANCOM-BC[108]. Data analysis was done in R (4.2). No custom code or software was used in data processing or analysis.

Reporting summary

Further information on research design is available in the Nature Portfolio Reporting Summary linked to this article.

Data availability

Sequence reads from the animal study are available at the Sequence Read Archive under Accession #SRP405883. Sequence reads for the human study are available from the Sequence Read Archive under BioProject #PRJNA725213. Source data for all Fig. are provided as supported data files. Source data are provided with this paper.

Code availability

Scripts to reproduce all findings shown in the main Fig. are available at https://github.com/amill017/kidney_bact.

References

1. Kim, M. M. et al. A scoping review of the economic burden of non-cancerous genitourinary conditions. *Urology* **166**, 29–38 (2022).
2. Dirks, J., Remuzzi, G., Horton, S., Schieppati, A. & Rizvi, S. A. H. in *Disease Control Priorities in Developing Countries* (eds D. T. Jamison, et al.) (2006).
3. Hilt, E. E. et al. Urine is not sterile: use of enhanced urine culture techniques to detect resident bacterial flora in the adult female bladder. *J. Clin. Microbiol* **52**, 871–876 (2014).
4. Shrestha, E. et al. Profiling the urinary microbiome in men with positive versus negative biopsies for prostate cancer. *J. Urol.* **199**, 161–171 (2018).
5. Bucevic Popovic, V. et al. The urinary microbiome associated with bladder cancer. *Sci. Rep.* **8**, 12157 (2018).
6. Fouts, D. E. et al. Integrated next-generation sequencing of 16S rDNA and metaproteomics differentiate the healthy urine microbiome from asymptomatic bacteriuria in neuropathic bladder associated with spinal cord injury. *J. Transl. Med* **10**, 174 (2012).
7. Zampini, A., Nguyen, A. H., Rose, E., Monga, M. & Miller, A. W. Defining dysbiosis in patients with urolithiasis. *Sci. Rep.* **9**, 5425 (2019).
8. Song, C. H. et al. Lactobacillus crispatus Limits Bladder Uropathogenic E. coli Infection by Triggering a Host Type I Interferon Response. *Proc. Natl Acad. Sci. USA* **119**, e2117904119 (2022).
9. Kachroo, N., Monga, M. & Miller, A. W. Comparative functional analysis of the urinary tract microbiome for individuals with or without calcium oxalate calculi. *Urolithiasis* **50**, 303–317 (2022).
10. Stapleton, A. E. et al. Randomized, placebo-controlled phase 2 trial of a Lactobacillus crispatus probiotic given intravaginally for prevention of recurrent urinary tract infection. *Clin. Infect. Dis.* **52**, 1212–1217 (2011).
11. He, Y. et al. Evaluation of the inhibitory effects of lactobacillus gasseri and lactobacillus crispatus on the adhesion of seven common lower genital tract infection-causing pathogens to vaginal epithelial cells. *Front Med (Lausanne)* **7**, 284 (2020).
12. Espinosa-Ortiz, E. J., Eisner, B. H., Lange, D. & Gerlach, R. Current insights into the mechanisms and management of infection stones. *Nat. Rev. Urol.* **16**, 35–53 (2019).
13. Zhong, F. et al. The characteristic and relationship of Escherichia coli isolated from urine and stones in patients with calcium oxalate stones. *Urolithiasis* **49**, 407–414 (2021).
14. Kaijser, B., Larsson, P. & Olling, S. Protection against ascending Escherichia coli pyelonephritis in rats and significance of local immunity. *Infect. Immun.* **20**, 78–81 (1978).
15. Kanlaya, R., Naruepantawart, O. & Thongboonkerd, V. Flagellum is responsible for promoting effects of viable escherichia coli on calcium oxalate crystallization, crystal growth, and crystal aggregation. *Front. Microbiol.* **10**, 2507 (2019).
16. Dornbier, R. A. et al. The microbiome of calcium-based urinary stones. *Urolithiasis* **48**, 191–199 (2020).
17. Barr-Beare, E. et al. The interaction between enterobacteriaceae and calcium oxalate deposits. *PLoS One* **10**, e0139575 (2015).
18. Hong, C. et al. Viral associations with kidney disease diagnosis and altered kidney metatranscriptome by kidney function. *Kidney Int.* **103**, 218–222 (2023).
19. Blaser, M. J. et al. Lessons learned from the prenatal microbiome controversy. *Microbiome* **9**, 8 (2021).
20. Xu, J. et al. The effect of different combinations of antibiotic cocktails on mice and selection of animal models for further microbiota research. *Appl Microbiol Biotechnol.* **105**, 1669–1681 (2021).
21. Karstens, L. et al. Does the urinary microbiome play a role in urgency urinary incontinence and its severity? *Front Cell Infect. Microbiol* **6**, 78 (2016).
22. Xie, J. et al. Profiling the urinary microbiome in men with calcium-based kidney stones. *BMC Microbiol.* **20**, 41 (2020).
23. Krych, L., Hansen, C. H., Hansen, A. K., van den Berg, F. W. & Nielsen, D. S. Quantitatively different, yet qualitatively alike: a meta-analysis of the mouse core gut microbiome with a view towards the human gut microbiome. *PLoS One* **8**, e62578 (2013).
24. Erb-Downward, J. R. et al. Analysis of the lung microbiome in the "healthy" smoker and in COPD. *PLoS One* **6**, e16384 (2011).
25. Murawski, I. J., Watt, C. L. & Gupta, I. R. Assessing urinary tract defects in mice: methods to detect the presence of vesicoureteric reflux and urinary tract obstruction. *Methods Mol. Biol.* **886**, 351–362 (2012).
26. Tasian, G., Miller, A. & Lange, D. Antibiotics and kidney stones: perturbation of the gut-kidney axis. *Am. J. Kidney Dis.* **74**, 724–726 (2019).

27. Schultz, L. N., Connolly, J., Lauchnor, E., Hobbs, T. A. & Gerlach, R. Struvite stone formation by ureolytic biofilm infections. *The Role of Bacteria in Urol.*, 41–49 (2016).
28. Werneburg, G. T. et al. Biofilms on indwelling artificial urinary sphincter devices harbor complex microbe-metabolite interaction networks and reconstitute differentially in vitro by material type. *Biomedicines* **11**, https://doi.org/10.3390/biomedicines11010215 (2023).
29. Werneburg, G. T. et al. Ureteral stents harbor complex biofilms with rich microbiome-metabolite interactions. *J. Urol.* **209**, 950–962 (2023).
30. Anisimova, E. A. & Yarullina, D. R. Antibiotic resistance of LACTOBACILLUS strains. *Curr. Microbiol* **76**, 1407–1416 (2019).
31. Iredell, J., Brown, J. & Tagg, K. Antibiotic resistance in Enterobacteriaceae: mechanisms and clinical implications. *BMJ* **352**, h6420 (2016).
32. Khan, S. R., Canales, B. K. & Dominguez-Gutierrez, P. R. Randall's plaque and calcium oxalate stone formation: role for immunity and inflammation. *Nat. Rev. Nephrol.* **17**, 417–433 (2021).
33. Menezes-Garcia, Z. et al. Colonization by Enterobacteriaceae is crucial for acute inflammatory responses in murine small intestine via regulation of corticosterone production. *Gut Microbes* **11**, 1531–1546 (2020).
34. Miller, A. W., Orr, T., Dearing, D. & Monga, M. Loss of function dysbiosis associated with antibiotics and high fat, high sugar diet. *ISME J.* **13**, 1379–1390 (2019).
35. Mulay, S. R. et al. Calcium oxalate crystals induce renal inflammation by NLRP3-mediated IL-1beta secretion. *J. Clin. Invest* **123**, 236–246 (2013).
36. Nielsen, R. et al. Repeated bronchoscopy in health and obstructive lung disease: is the airway microbiome stable? *BMC Pulm. Med* **21**, 342 (2021).
37. Zaneveld, J. R., McMinds, R. & Vega Thurber, R. Stress and stability: applying the Anna Karenina principle to animal microbiomes. *Nat. Microbiol* **2**, 17121 (2017).
38. Karstrup, C. C., Klitgaard, K., Jensen, T. K., Agerholm, J. S. & Pedersen, H. G. Presence of bacteria in the endometrium and placentomes of pregnant cows. *Theriogenology* **99**, 41–47 (2017).
39. Chen, L. et al. Influence of Bacillus subtilis on the growth of calcium oxalate. *Cryst. Res. Technol.: J. Exp. Ind. Crystallogr.* **42**, 881–885 (2007).
40. Hobbs, T., Schultz, L. N., Lauchnor, E. G., Gerlach, R. & Lange, D. Evaluation of biofilm induced urinary infection stone formation in a novel laboratory model system. *J. Urol.* **199**, 178–185 (2018).
41. Liu, N. et al. Shape and structure controlling of calcium oxalate crystals by a combination of additives in the process of biomineralization. *RSC Adv.* **8**, 11014–11020 (2018).
42. Wesson, J. A., Worcester, E. M., Wiessner, J. H., Mandel, N. S. & Kleinman, J. G. Control of calcium oxalate crystal structure and cell adherence by urinary macromolecules. *Kidney Int* **53**, 952–957 (1998).
43. Ruiz-Agudo, E. et al. A non-classical view on calcium oxalate precipitation and the role of citrate. *Nat. Commun.* **8**, 768 (2017).
44. Rusakov, A., Kuz'mina, M. & Frank-Kamenetskaya, O. Biofilm medium chemistry and calcium oxalate morphogenesis. *Molecules* **26**, 10.3390/molecules26165030 (2021).
45. Lekcharoensuk, C. et al. Association between dietary factors and calcium oxalate and magnesium ammonium phosphate urolithiasis in cats. *J. Am. Vet. Med. Assoc.* **219**, 1228–1237 (2001).
46. Lekcharoensuk, C. et al. Associations between dry dietary factors and canine calcium oxalate uroliths. *Am. J. Vet. Res.* **63**, 330–337 (2002).
47. Landry, G. M. et al. Sulfate and thiosulfate inhibit oxalate transport via a dPrestin (Slc26a6)-dependent mechanism in an insect model of calcium oxalate nephrolithiasis. *Am. J. Physiol. Ren. Physiol.* **310**, F152–F159 (2016).
48. Rodgers, A. et al. Sulfate but not thiosulfate reduces calculated and measured urinary ionized calcium and supersaturation: implications for the treatment of calcium renal stones. *PloS one* **9**, e103602 (2014).
49. Finlayson, B. & Roth, R. Appraisal of calcium oxalate solubility in sodium chloride and sodium-calcium chloride solutions. *Urology* **1**, 142–144 (1973).
50. Selvam, R. & Kalaiselvi, P. Oxalate binding proteins in calcium oxalate nephrolithiasis. *Urol. Res* **31**, 242–256 (2003).
51. Atakan, I. H. et al. Serum, urinary and stone zinc, iron, magnesium and copper levels in idiopathic calcium oxalate stone patients. *Int Urol. Nephrol.* **39**, 351–356 (2007).
52. Sheng, X. et al. Mapping the genetic architecture of human traits to cell types in the kidney identifies mechanisms of disease and potential treatments. *Nat. Genet* **53**, 1322–1333 (2021).
53. Karstens, L. et al. Controlling for contaminants in low-biomass 16S rRNA gene sequencing experiments. *mSystems* **4,** 10.1128/mSystems.00290-19 (2019).
54. Salter, S. J. et al. Reagent and laboratory contamination can critically impact sequence-based microbiome analyses. *BMC Biol.* **12**, 1–12 (2014).
55. Behzadi, P. et al. A survey on urinary tract infections associated with the three most common uropathogenic bacteria. *Maedica (Bucur.)* **5**, 111–115 (2010).
56. Bao, Y. et al. Questions and challenges associated with studying the microbiome of the urinary tract. *Ann. Transl. Med* **5**, 33 (2017).
57. Johnson, J. R. & Manivel, J. C. Vesicoureteral reflux induces renal trauma in a mouse model of ascending, unobstructed pyelonephritis. *J. Urol.* **145**, 1306–1311 (1991).
58. Mittal, R. et al. Experimental non-obstructive chronic renal infection model with planktonic and biofilm cells of Pseudomonas aeruginosa. *Am. J. Biomed. Sci.* **1**, 103–114 (2009).
59. Sharma, K., Bose, S. K., Chhibber, S. & Harjai, K. Exploring the therapeutic efficacy of zingerone nanoparticles in treating biofilm-associated pyelonephritis caused by Pseudomonas aeruginosa in the murine model. *Inflammation* **43**, 2344–2356 (2020).
60. Linh, H. T. et al. Intestinal bacterial translocation contributes to diabetic kidney disease. *J. Am. Soc. Nephrol.* **33**, 1105–1119 (2022).
61. Sullivan, M. J. & Ulett, G. C. Evaluation of hematogenous spread and ascending infection in the pathogenesis of acute pyelonephritis due to group B streptococcus in mice. *Micro Pathog.* **138**, 103796 (2020).
62. Xiang, X., Poli, D., Degnan, B. M. & Degnan, S. M. Ribosomal RNA-depletion provides an efficient method for successful dual rna-seq expression profiling of a marine sponge holobiont. *Mar. Biotechnol. (NY)* **24**, 722–732 (2022).
63. Blazewicz, S. J., Barnard, R. L., Daly, R. A. & Firestone, M. K. Evaluating rRNA as an indicator of microbial activity in environmental communities: limitations and uses. *ISME J.* **7**, 2061–2068 (2013).
64. Ahmadi, S. et al. A human-origin probiotic cocktail ameliorates aging-related leaky gut and inflammation via modulating the microbiota/taurine/tight junction axis. *JCI insight* **5** (2020).
65. Martin, J. & Sheaff, M. Renal ageing. *J. Pathol.: A J. Pathological Soc. Gt. Br. Irel.* **211**, 198–205 (2007).
66. Yap, H.-K. & Lau, P. Y.-W. in *Pediatric kidney disease* 373–404 (Springer, 2023).
67. Bratzler, D. W. et al. Clinical practice guidelines for antimicrobial prophylaxis in surgery. *Surg. Infect. (Larchmt.)* **14**, 73–156 (2013).
68. Tasian, G. E. et al. Oral antibiotic exposure and kidney stone disease. *J. Am. Soc. Nephrol.* **29**, 1731–1740 (2018).
69. Walton, K., Dorne, J. L. & Renwick, A. G. Species-specific uncertainty factors for compounds eliminated principally by renal excretion in humans. *Food Chem. Toxicol.* **42**, 261–274 (2004).

70. Kachroo, N. et al. Meta-analysis of clinical microbiome studies in urolithiasis reveal age, stone composition, and study location as the predominant factors in urolithiasis-associated microbiome composition. *mBio* **12**, e0200721 (2021).
71. Saxena, V. et al. Kidney intercalated cells are phagocytic and acidify internalized uropathogenic Escherichia coli. *Nat. Commun.* **12**, 2405 (2021).
72. Wu, P. et al. Urinary microbiome and psychological factors in women with overactive bladder. *Front Cell Infect. Microbiol* **7**, 488 (2017).
73. Knoop, K. A., McDonald, K. G., Kulkarni, D. H. & Newberry, R. D. Antibiotics promote inflammation through the translocation of native commensal colonic bacteria. *Gut* **65**, 1100–1109 (2016).
74. Djojodimedjo, T., Soebadi, D. M. & Soetjipto Escherichia coli infection induces mucosal damage and expression of proteins promoting urinary stone formation. *Urolithiasis* **41**, 295–301 (2013).
75. Wang, X. et al. Distinguishing characteristics of idiopathic calcium oxalate kidney stone formers with low amounts of Randall's plaque. *Clin. J. Am. Soc. Nephrol.* **9**, 1757–1763 (2014).
76. Falah, F. et al. Evaluation of adherence and anti-infective properties of probiotic Lactobacillus fermentum strain 4-17 against Escherichia coli causing urinary tract infection in humans. *Micro Pathog.* **131**, 246–253 (2019).
77. Chutipongtanate, S., Sutthimethakorn, S., Chiangjong, W. & Thongboonkerd, V. Bacteria can promote calcium oxalate crystal growth and aggregation. *JBIC. J. Biol. Inorg. Chem.* **18**, 299–308 (2013).
78. Rimer, J. D., Kolbach-Mandel, A. M., Ward, M. D. & Wesson, J. A. The role of macromolecules in the formation of kidney stones. *Urolithiasis* **45**, 57–74 (2017).
79. Yoshihara, A. et al. Estimation of the adhesive force distribution for the flagellar adhesion of Escherichia coli on a glass surface. *Colloids Surf. B Biointerfaces* **131**, 67–72 (2015).
80. Clark, R., Campbell, A., Klumb, L., Long, C. & Stayton, P. Protein electrostatic surface distribution can determine whether calcium oxalate crystal growth is promoted or inhibited. *Calcif. tissue Int.* **64**, 516–521 (1999).
81. Nearing, J. T. et al. Microbiome differential abundance methods produce different results across 38 datasets. *Nat. Commun.* **13**, 342 (2022).
82. Eisenhofer, R. et al. Contamination in low microbial biomass microbiome studies: issues and recommendations. *Trends Microbiol* **27**, 105–117 (2019).
83. Rabstein, L., Peters, R. & Spahn, G. Spontaneous tumors and pathologic lesions in SWR/J mice. *J. Natl Cancer Inst.* **50**, 751–758 (1973).
84. Hoogstraten-Miller, S. L. & Brown, P. A. Techniques in aseptic rodent surgery. *Curr. Protoc. Immunol.* **82**, 1.12. 11–11.12. 14 (2008).
85. Brooks, T. & Keevil, C. W. A simple artificial urine for the growth of urinary pathogens. *Lett. Appl Microbiol* **24**, 203–206 (1997).
86. Livak, K. J. & Schmittgen, T. D. Analysis of relative gene expression data using real-time quantitative PCR and the 2− ΔΔCT method. *methods* **25**, 402–408 (2001).
87. Suzuki, M. T., Taylor, L. T. & DeLong, E. F. Quantitative analysis of small-subunit rRNA genes in mixed microbial populations via 5′-nuclease assays. *Appl Environ. Microbiol* **66**, 4605–4614 (2000).
88. Stedtfeld, R. D. et al. Primer set 2.0 for highly parallel qPCR array targeting antibiotic resistance genes and mobile genetic elements. *FEMS Microbiol. Ecol.* **94**, fiy130 (2018).
89. Seemann, T. Prokka: rapid prokaryotic genome annotation. *Bioinformatics* **30**, 2068–2069 (2014).
90. Miller, A. W., Kohl, K. D. & Dearing, M. D. The gastrointestinal tract of the white-throated woodrat (Neotoma albigula) harbors distinct consortia of oxalate-degrading bacteria. *Appl. Environ. Microbiol.* **80**, 1595–1601 (2014).
91. Daims, H., Brühl, A., Amann, R., Schleifer, K.-H. & Wagner, M. The domain-specific probe EUB338 is insufficient for the detection of all Bacteria: development and evaluation of a more comprehensive probe set. *Syst. Appl. Microbiol.* **22**, 434–444 (1999).
92. Raghavulu, S. V., Modestra, J. A., Amulya, K., Reddy, C. N. & Mohan, S. V. Relative effect of bioaugmentation with electrochemically active and non-active bacteria on bioelectrogenesis in microbial fuel cell. *Bioresour. Technol.* **146**, 696–703 (2013).
93. Quevedo, B. et al. Phylogenetic group-and species-specific oligonucleotide probes for single-cell detection of lactic acid bacteria in oral biofilms. *BMC Microbiol.* **11**, 1–12 (2011).
94. Jensen, H. E. et al. Fluorescence in situ hybridization for the tissue detection of bacterial pathogens associated with porcine infections. *Veterinary infection biology: Molecular diagnostics and high-throughput strategies*, 219–234 (2015).
95. De Nisco, N. J. et al. Direct detection of tissue-resident bacteria and chronic inflammation in the bladder wall of postmenopausal women with recurrent urinary tract infection. *J. Mol. Biol.* **431**, 4368–4379 (2019).
96. Schmidt, K. et al. Identification of bacterial pathogens and antimicrobial resistance directly from clinical urines by nanopore-based metagenomic sequencing. *J. Antimicrobial Chemother.* **72**, 104–114 (2016).
97. Caporaso, J. G. et al. Ultra-high-throughput microbial community analysis on the Illumina HiSeq and MiSeq platforms. *ISME J.* **6**, 1621–1624 (2012).
98. Grigoriev, I. V. et al. The genome portal of the department of energy joint genome institute. *Nucleic acids Res.* **40**, D26–D32 (2012).
99. Li, H. Aligning sequence reads, clone sequences and assembly contigs with BWA-MEM. *arXiv preprint arXiv:1303.3997* (2013).
100. Team, R. C. R: A language and environment for statistical computing. R Foundation for Statistical Computing. *(No Title)* (2013).
101. Callahan, B. J. et al. High-throughput amplicon sequencing of the full-length 16S rRNA gene with single-nucleotide resolution. *Nucleic acids Res.* **47**, e103–e103 (2019).
102. Quast, C. et al. The SILVA ribosomal RNA gene database project: improved data processing and web-based tools. *Nucleic acids Res.* **41**, D590–D596 (2012).
103. Federhen, S. The NCBI taxonomy database. *Nucleic acids Res.* **40**, D136–D143 (2012).
104. Oksanen, J. vegan: Community Ecology Package-R package version 1.17-8. http://CRAN.R-project.org/package=vegan (2011).
105. Bodenhofer, U., Bonatesta, E., Horejš-Kainrath, C. & Hochreiter, S. msa: an R package for multiple sequence alignment. *Bioinformatics* **31**, 3997–3999 (2015).
106. Love, M. I., Huber, W. & Anders, S. Moderated estimation of fold change and dispersion for RNA-seq data with DESeq2. *Genome Biol.* **15**, 1–21 (2014).
107. Lin, H. & Peddada, S. D. Analysis of compositions of microbiomes with bias correction. *Nat. Commun.* **11**, 3514 (2020).
108. Cappellato, M., Baruzzo, G. & Di Camillo, B. Investigating differential abundance methods in microbiome data: A benchmark study. *PLoS Computational Biol.* **18**, e1010467 (2022).

Acknowledgements

We appreciate the technical support from John Peterson and Ajay Zalavadia from the Imaging Core of the Lerner Research Institute for their support in FISH experiments, SEM and EDS procedures and interpretation. We thank Mangesh Suryavanshi for his help to test VUR phenotype in SWR/J mice. This work was supported by Urology Care Foundation 2020 Research Scholar Award Program (UCF2020-JA,

Cleveland Clinic Research Programs Committees (RPC 307- AWM), and National Institute of Health (R01DK121689 - AWM).

Author contributions

J.A. and A.M. conceived and designed the study, and conducted the animal and in vitro studies. X.C. and J.A. performed the FISH analysis. S.M. conducted the qRT-PCR analysis. L.B. and J.N. oversaw the processing and access to kidney human tissue and provided support for the FISH analysis in these samples. J.A. and A.M. wrote the manuscript with input from X.C., S.M., and J.N.

Competing interests

The authors declare no competing interests.

Additional information

Supplementary information The online version contains supplementary material available at https://doi.org/10.1038/s41467-024-54432-6.

Correspondence and requests for materials should be addressed to Jose Agudelo.

Peer review information *Nature Communications* thanks Andrew Schwaderer, and the other, anonymous, reviewer for their contribution to the peer review of this work. A peer review file is available.